ORNL/SUB/00-XSZ175V-1

OAK RIDGE NATIONAL LABORATORY

LOCKHEED MARTIN

Neutronics Benchmarks for the Utilization of Mixed-Oxide Fuel: Joint U.S./Russian Progress Report for Fiscal Year 1997

Volume 4, Part 5—ESADA Plutonium Program Critical Experiments: Multiregion Core Configurations

Hatice Akkurt
Naeem M. Abdurrahman

Fissile Materials Disposition Program

MANAGED AND OPERATED BY
LOCKHEED MARTIN ENERGY RESEARCH CORPORATION
FOR THE UNITED STATES
DEPARTMENT OF ENERGY

ORNL-27 (3-96)

Available electronically from the following source:

Web site www.doe.gov/bridge

Reports are available in paper to the public from the following source.

U.S. Department of Commerce
National Technical Information Service
5285 Port Royal Road
Springfield, VA 22161
Telephone 1-800-553-6847
TDD 703-487-4639
Fax 703-605-6900
E-mail orders@ntis.fedworld.gov
Web site www.ntis.gov/ordering.htm

Reports are available in paper to U.S. Department of Energy (DOE) employees, DOE contractors, Energy Technology Data Exchange (ETDE) representatives, and International Nuclear Information System (INIS) representatives from the following source.

Office of Scientific and Technical Information
P.O. Box 62
Oak Ridge, TN 37831
Telephone 865-576-8401
Fax 865-576-5728
E-mail reports@adonis.osti.gov

This report was prepared as an account of work sponsored by an agency of the United States Government. Neither the United States Government nor any agency thereof, nor any of their employees, makes any warranty, express or implied, or assumes any legal liability or responsibility for the accuracy, completeness, or usefulness or any information, apparatus, product, or process disclosed, or represents that its use would not infringe privately owned rights. Reference herein to any specific commercial product, process, or service by trade name, trademark, manufacturer, or otherwise, does not necessarily constitute or imply its endorsement, recommendation, or favoring by the United States Government or any agency thereof. The views and opinions of authors expressed herein do not necessarily state or reflect those of the United States Government or any agency thereof.

ORNL/SUB/00-XSZ175V-1

Neutronics Benchmarks for the Utilization of Mixed-Oxide Fuel: Joint U.S./Russian Progress Report for Fiscal Year 1997

Volume 4, Part 5—ESADA PLUTONIUM PROGRAM CRITICAL EXPERIMENTS: MULTIREGION CORE CONFIGURATIONS

Hatice Akkurt
Naeem M. Abdurrahman

Date Published: February 2000

Report Prepared by
LOCKHEED MARTIN ENERGY RESEARCH CORP.
P.O. Box 2008
Oak Ridge, Tennessee 37831-6363
under
Subcontract Number 85B99398V

Funded by
Office of Fissile Materials Disposition
U.S. Department of Energy

Prepared for
Computational Physics and Engineering Division
OAK RIDGE NATIONAL LABORATORY
Oak Ridge, Tennessee 37831
managed by
LOCKHEED MARTIN ENERGY RESEARCH CORP.
for the
U.S. DEPARTMENT OF ENERGY
under contract DE-AC05-96OR22464

FINAL REPORT

ESADA PLUTONIUM PROGRAM CRITICAL EXPERIMENTS: MULTIREGION CORE CONFIGURATIONS

Hatice Akkurt and Naeem M. Abdurrahman

College of Engineering

Department of Mechanical Engineering

University of Texas

Austin, TX 78712

February 1999

CONTENTS

Page

LIST OF TABLES v
LIST OF FIGURES vii
1. DETAILED DESCRIPTION 1
1.1 Overview of Experiment 1
1.2 Description of Experimental Configuration 1
1.2.1 Types of Measurements 4
1.2.2 Critical Experiments with Salt-and-Pepper Core Configurations 5
1.2.3 Critical Experiments with Concentric-Region Core Configurations 15
1.2.4 Critical Experiments with Multiregion Slab Core Configurations 26
1.3 Description of Fuel Rods 36
1.4 Description of Test Configurations 37
1.5 Description of Materials 38
1.6 Supplemental Experimental Measurements 42
2. EVALUATION OF THE EXPERIMENTAL DATA 44
3. BENCHMARK SPECIFICATIONS 46
3.1 Description of Model 46
3.2 Dimensions 46
3.3 Material Data 45
3.4 Temperature Data 49
4. RESULTS OF CALCULATIONS 51
5. REFERENCES 53

LIST OF TABLES

Table		Page
1	Reported data for salt-and-pepper configurations	7
2	Reported data for concentric-region core configurations	17
3	Reported data for multiregion slab core configurations	28
4	MOX and UO_2 fuel rod specifications	37
5	Isotopic composition of the metal plutonium in the MOX fuel rods	38
6	Percentages of the elements in the MOX fuel rods	38
7	Zircaloy-2 composition used for MOX fuel	38
8	Chemical analysis of UO_2 fuel	40
9	Chemical analysis of Zircaloy-4 clad used for UO_2 fuel	41
10	Isotopic distribution of Al-6061	41
11	Isotopic composition of Ag-In-Cd control rod	41
12	Atomic densities for the 8 wt % and 24 wt % ^{240}Pu MOX fuels	47
13	Atomic densities for the UO_2 powder at the top of the MOX fuels	47
14	Atomic densities for the Zircaloy-2 clad used for MOX fuel	48
15	Atomic densities for the UO_2 fuel	48
16	Atomic densities for the Zircaloy-4 clad	48
17	Atomic densities for the Al-6061	49
18	Atomic densities for water	49
19	Atomic densities for 526 ppm borated water	49
20	Atomic densities for air	49
21	Atomic densities for the control rod	49
22	MCNP calculation results for salt-and-pepper core configurations	51
23	MCNP results for concentric-region core configurations	51
24	MCNP calculation results for multiregion slab core configurations	52

LIST OF FIGURES

Figure		Page
1	Installation of MOX fuel in uniform lattice	2
2	Installation of salt-and-pepper core	3
3	Installation of multiregion core	4
4	Salt-and-pepper core configuration	6
5	A 27×27 salt-and-pepper core configuration composed of 8 wt % ^{240}Pu and UO_2 with uniformly distributed nine-rod pattern in a 1.7526-cm lattice	8
6	A 27×27 salt-and-pepper core configuration composed of 8 wt % ^{240}Pu and 24 wt % ^{240}Pu fuels	9
7	A 23×23 salt-and-pepper core configuration composed of 8 wt % ^{240}Pu and UO_2 fuels	10
8	A 23×23 salt-and-pepper core configuration composed of 24 wt % ^{240}Pu and UO_2 fuels	11
9	A 24×24 salt-and-pepper core configuration composed of 24 wt % ^{240}Pu and UO_2 fuels	12
10	A 25×25 salt-and-pepper core configuration composed of 24 wt % ^{240}Pu and UO_2 fuels	13
11	A cylindrical salt-and-pepper core configuration composed of 24 wt % ^{240}Pu and UO_2 fuels	14
12	The concentric-region core configuration with MOX fuel in the inner region and UO_2 fuel in the outer region	16
13	A 25×25 concentric-region core configuration containing a 15×15, 8 wt % ^{240}Pu, inner region and UO_2 outer region	18
14	A 25×25 concentric-region core configuration containing a 15×15, UO_2 inner region and 24 wt % ^{240}Pu outer region	19
15	A 25×25 concentric-region core configuration containing a 15×15, 24 wt % ^{240}Pu, inner region and UO_2 outer region	20
16	A 23×23 concentric-region core configuration containing an 11×11, 24 wt % ^{240}Pu, inner region and UO_2 outer region	21
17	A 27×27 concentric-region core configuration containing a 15×15, 24 wt % ^{240}Pu, inner region and 8 wt % ^{240}Pu outer region	22
18	A cylindrical concentric-region core configuration containing a 24 wt % ^{240}Pu inner region and an 8 wt % ^{240}Pu outer region	23
19	A cylindrical concentric-region core configuration containing a 24 wt % ^{240}Pu inner region and an 8 wt % ^{240}Pu outer region	24
20	A cylindrical concentric-region core configuration containing a 24 wt % ^{240}Pu inner region and an 8 wt % ^{240}Pu outer region with a regional variation in lattice pitch	25
21	Multiregion core configuration with the UO_2 slabs sandwiching MOX in central region	26
22	Multiregion core configuration with alternating rows of 8 wt % and 24 wt % ^{240}Pu MOX in the central region and UO_2 fuel in the outer regions	27
23	A multiregion core configuration with traverse slabs of 8 wt % ^{240}Pu and 24 wt % ^{240}Pu MOX in the central region and UO_2 fuel in the outer region	27
24	A multiregion core configuration with a 4×4 local void simulation using aluminum tubes	28
25	The multiregion slab core configuration containing an 8 wt % ^{240}Pu central region (19×19) and UO_2 outer regions (10×23) with a 4×4 central void pattern	29
26	A multiregion slab core configuration containing an 8 wt % ^{240}Pu central region (19×19) and UO_2 outer regions (10×23) with a 10×10 central void pattern	30

27 A multiregion slab reference core configuration containing an 8 wt % ^{240}Pu central region (19 × 23) and UO_2 outer regions (15 × 27) 31
28 A multiregion slab core configuration containing an 8 wt % ^{240}Pu central region (19 × 23) and UO_2 outer regions (15 × 27) with a 10 × 10 central void pattern 32
29 A multiregion slab core configuration containing an 8 wt % ^{240}Pu central region (19 × 23) and UO_2 outer regions (15 × 27) with a 4 × 4 central void pattern 33
30 A multiregion slab core configuration containing central traverse slabs of 8 wt % ^{240}Pu and 24 wt % ^{240}Pu fuels (19 × 21) and UO_2 outer regions (10 × 25) 34
31 A multiregion slab core configuration containing alternate rows of 8 wt % ^{240}Pu and 24 wt % ^{240}Pu fuels in the central slab region (19 × 21) and UO_2 outer regions (10 × 25) 35
32 MOX fuel rod 36
33 Uranium fuel rod 37

ESADA PLUTONIUM PROGRAM CRITICAL EXPERIMENTS: MULTIREGION CORE CONFIGURATIONS*†

Hatice Akkurt
Naeem M. Abdurrahman

1. DETAILED DESCRIPTION

1.1 Overview of Experiment

In 1967, a series of critical experiments were conducted at the Westinghouse Reactor Evaluation Center (WREC) using mixed-oxide (MOX) PuO_2-UO_2 and/or UO_2 fuels in various lattices and configurations[1]. These experiments were performed under the joint sponsorship of the Empire State Atomic Development Associates (ESADA) plutonium program and Westinghouse[2]. The purpose of these experiments was to develop experimental data to validate analytical methods used in the design of a plutonium-bearing replacement fuel for water reactors.

Three different fuels were used during the experimental program: two MOX fuels and a low-enriched UO_2 fuel. The MOX fuels were distinguished by their ^{240}Pu content: 8 wt % ^{240}Pu and 24 wt % ^{240}Pu. Both MOX fuels contained 2.0 wt % PuO_2 in natural UO_2. The UO_2 fuel with 2.72 wt % enrichment was used for comparison with the plutonium data and for use in multiregion experiments.

1.2 Description of Experimental Configuration

A total of 88 different critical core configurations were constructed for the experimental program. Both single-region and multiregion core configurations were used in the ESADA experiments. These core configurations were constructed by changing the lattice pitch, fuel configuration, and fuel isotopic composition. All experiments were performed in a ~112-cm-diam pool. Criticality was achieved by adjusting the height of the light-water moderator in the pool.

Fifty-three of these experiments were performed for single-region core configurations. The description and benchmark calculation results for single-region ESADA experiments are provided in Ref. 3.

Thirty-five of these experiments were performed for multiregion core configurations. Reactivity worth and power distribution measurements were performed using multiregion core configurations. During the power distribution measurements for the multiregion slab core configurations, vertical-buckling measurements were also performed in each region for each configuration.

The multiregion core configurations were constructed in three ways: concentric-region core configurations, salt-and-pepper core configurations, and a third configuration that can be generally described as two rectangular slabs loaded with UO_2, sandwiching a center region loaded with MOX fuel.

Concentric-region core configurations were constructed by using two different fuels in the inner and outer regions of the core. Salt-and-pepper core configurations were constructed by loading two different fuels in a checkerboard pattern. Various combinations of the available fuels were used during the core construction.

---

*__IDENTIFICATION NUMBERS.__ Configurations with no boron in the moderator are designated, collectively, in the International Handbook of Evaluated Criticality Safety Benchmark Experiments Project as MIX-COMP-THERM-010. Configurations with boron in the moderator are designated, collectively, as MIX-COMP-THERM-011.

†__KEY WORDS:__ critical experiments, mixed-oxide, MOX, plutonium, plutonium dioxide, PuO_2, water reactor, natural uranium, enriched uranium, UO_2, ESADA, Westinghouse, WREC, salt-and-pepper, concentric-region, multiregion core.

The MOX and UO_2 fuel rods have different diameters. In the concentric-region and salt-and-pepper core configurations, MOX and UO_2 fuel rods were used in the same lattice pitch. Therefore, for these cases with the same lattice pitches, different moderator-to-fuel volume ratios were obtained in the same configuration. Because the dimensions of both MOX fuels were the same, the moderator-to-fuel ratio was the same for the core configurations composed of these fuels. However, in one concentric-region core configuration, the MOX fuel in the outer region was loaded on the diagonal; thus, a variation in the fuel-to-moderator ratio was introduced for the configuration composed of MOX fuels as well.

For the third configuration, each of the cores consisted of two UO_2 slabs, sandwiching a center plutonium-fueled slab. The different diameters of the MOX and uranium fuel rods required that the lattices in the UO_2-fueled region and the MOX-fueled region have different pitches in order to have the same moderator-to-fuel ratio in each region.

For the multiregion core configurations composed of two different MOX fuels, installation of the core is given in Fig. 1. Installations of MOX and UO_2 fuels for salt-and-pepper and multiregion slab arrays are given in Figs. 2 and 3, respectively.

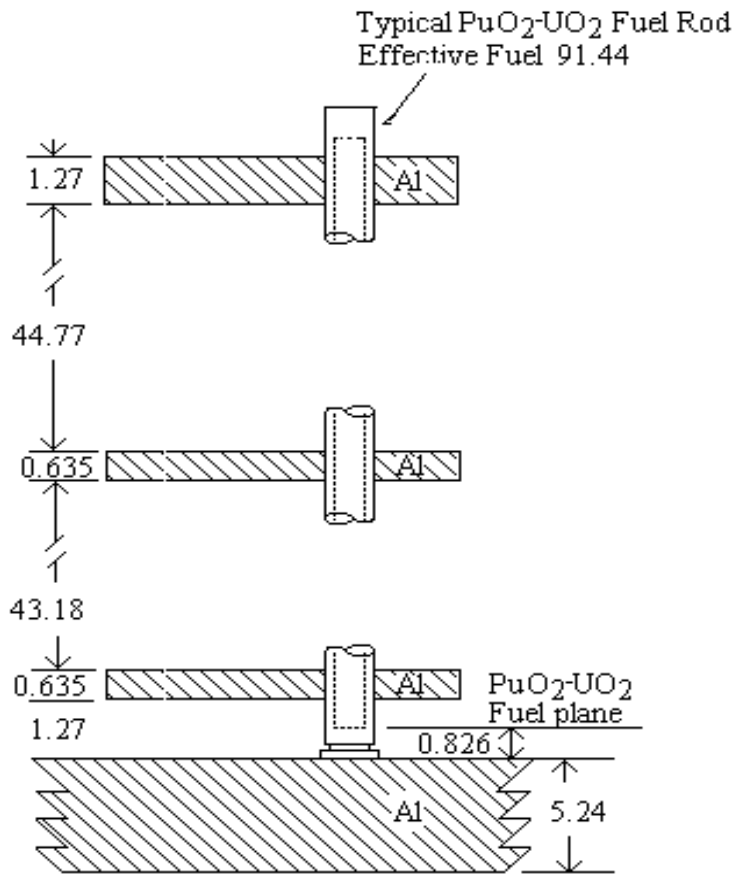

Fig. 1. Installation of MOX fuel in a uniform lattice. (Not drawn to scale; units are in centimeters except where specified otherwise.)

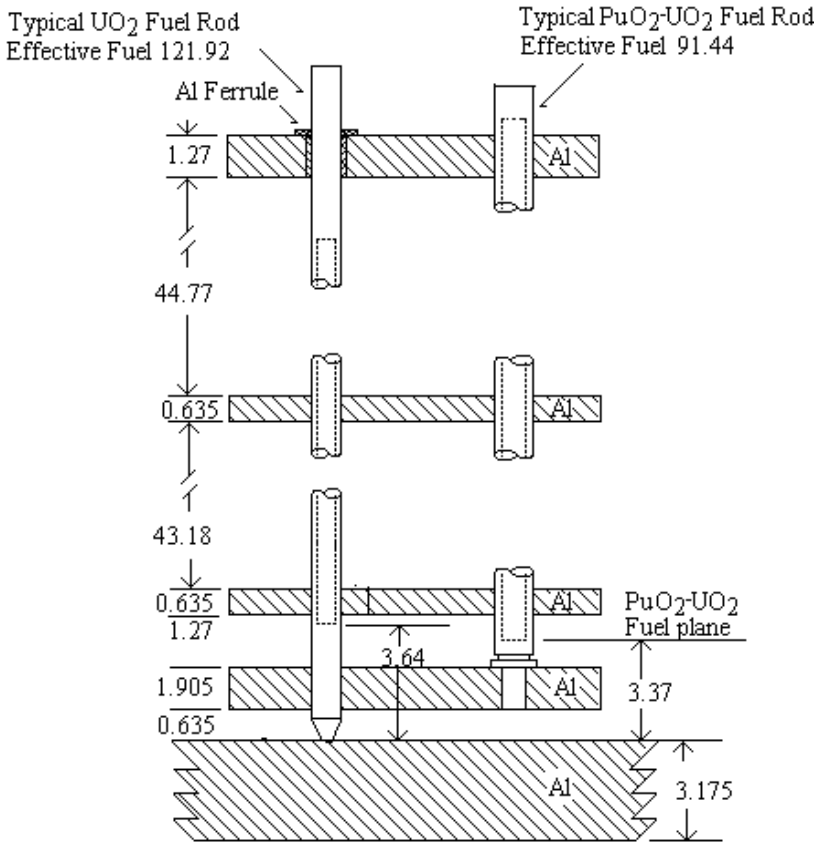

Fig. 2. Installation of salt-and-pepper core. (Not drawn to scale; units are in centimeters except where specified otherwise.)

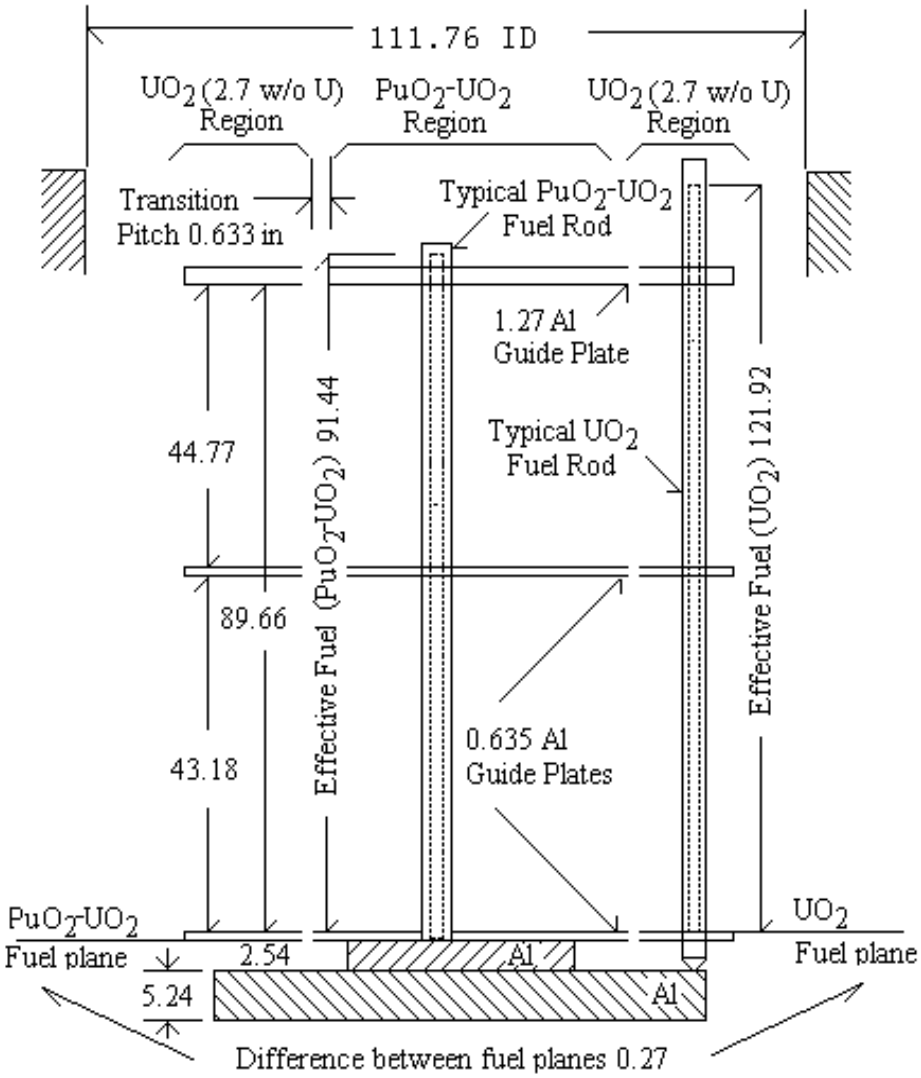

Fig. 3. Installation of the multiregion core. (Not drawn to scale; units are in centimeters except where specified otherwise.)

1.2.1 Types of Measurements

Measurements in the ESADA experimental program with multiregion core configurations can be summarized as follows:

1. The reactivity worth of different materials was measured in various test configurations for multiregion core configurations. Several test positions were formed by removing fuel rods. These holes were either filled with control rods or left as empty water holes. The reactivity effects of nine bare silver-indium-cadmium (Ag-In-Cd) rods and nine water holes in a uniformly distributed pattern were measured in a salt-and-pepper core that was composed of 8 wt % ^{240}Pu fuel and 2.72 wt % UO_2 fuel in a 1.7526-cm. lattice. The reactivity effect of local voids was measured in both clean and borated multiregion slab cores composed of 8 wt % ^{240}Pu fuel and 2.72 wt % UO_2 fuel. Sealed aluminum tubes were used to provide the voids. The aluminum tubes were inserted in holes drilled interstitially in the core plates and arranged in regions of varying size to simulate local voiding. Reactivity worths were obtained by

measuring the critical water heights of the reference and perturbed cores and integrating the differential water worth curve between the measured water heights.

2. Power distribution measurements were made for all three multiregion core configurations. Measurements were made by relating the fission product gamma activity of irradiated fuel rods to the temperature rise of the fuel-clad surface, which is proportional to the rod power.

1.2.2 Critical Experiments with Salt-and-Pepper Core Configurations

Salt-and-pepper core configurations were constructed by loading two different fuels in a checkerboard pattern. All available fuel types were used in various combinations for the salt-and-pepper core configurations. Reactivity and power distribution measurements were performed for this core configuration for clean cores. All experiments were performed in a 1.7526-cm lattice pitch.

The reactivity effects of nine bare Ag-In-Cd rods and nine water holes in a uniformly distributed pattern were measured in a salt-and-pepper core that was composed of 8 wt % ^{240}Pu fuel and 2.72 wt % UO_2 fuel.

Power distribution measurements were performed for six configurations with several combinations of fuel. One configuration was composed of 8 wt % ^{240}Pu fuel and 2.72 wt % UO_2 fuel, four configurations were composed of 24 wt % ^{240}Pu fuel and 2.72 wt % UO_2 fuel, and another configuration composed of 8 wt % ^{240}Pu fuel and 24 wt % ^{240}Pu fuel.

The MOX and UO_2 fuel rods had different diameters. In the salt-and-pepper core configurations, MOX and UO_2 fuels were used in the same lattice pitch. Therefore, with the same lattice pitches, different moderator-to-fuel volume ratios were obtained in the same core configuration. Because the dimensions of both MOX fuels were the same for the core configurations composed of these fuels, the moderator-to-fuel ratio was the same.

Installation of the MOX and the UO_2 fuel rods in a salt-and-pepper core configuration is illustrated in Fig. 2. The UO_2 fuel rods rested on a 5.24-cm aluminum plate. The height of UO_2 and MOX fuels differed. The MOX fuel rested on an aluminum plate with thickness of 1.9050 cm, and there was a 0.635-cm space available between these two aluminum plates. Both fuel rods were supported by three layers of aluminum plates. The thickness of bottom and central aluminum plates was 0.635-cm, and the thickness of the top aluminum plate was 1.27 cm. For salt-and-pepper core configurations composed of 8 wt % and 24 wt % ^{240}Pu fuels, single-region MOX fuel installation is used. Installation of MOX fuel is shown in Fig. 1. Fuel rods were supported by three layers of aluminum plates. The thickness of the bottom and midcore plates was 0.635 cm, and the thickness of the top plate was 1.27 cm. Fuel rods rested on a 5.24-cm-thick aluminum plate.

A photo of a salt-and-pepper core configuration is presented in Fig. 4. Reported data for salt-and-pepper core configurations are listed in Table 1. Schematic representations of core configurations are given in Figs. 5–11. For the schematic representation of the core configurations, the cross-section from the aluminum plate is taken as the reference plane. In these figures, the caption “hole” represents the fuel rod holes in the aluminum plate. These holes were filled with water. Information for core diagram numbers and measurement types are also included in Table 1.

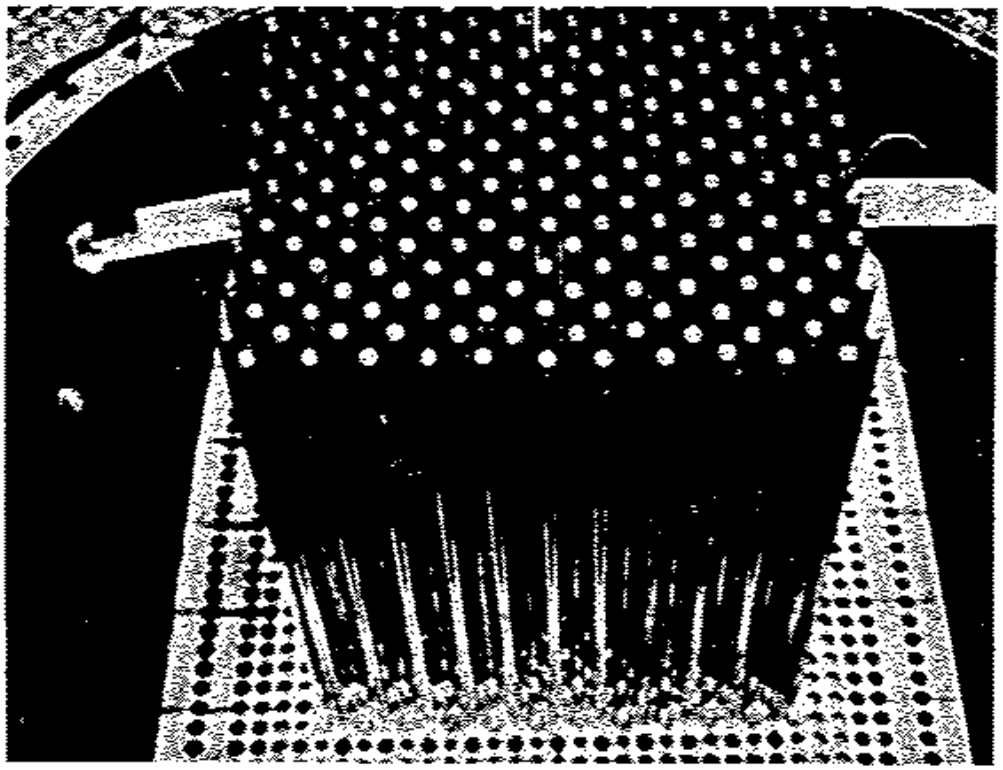

Fig. 4. Salt-and-pepper core configuration.

Table 1. Reported data for salt-and-pepper configurations[a,b]

Case No.	Core diagram (figure number)	Measurement type	Number of fuel rods	Critical water height (cm)	Test configuration
1	—	Reactivity	729 (365 8 wt % ^{240}Pu) (364 UO_2)	37.05	Reference core
2	5	Reactivity	720 (356 8 wt % ^{240}Pu) (364 UO_2)	36.65	Nine uniformly distributed water holes
3	5	Reactivity	720 (356 8 wt % ^{240}Pu) (364 UO_2)	43.42	Nine uniformly distributed Ag-In-Cd rods
4	6	Power distribution	729 (365 8 wt % ^{240}Pu) (364 24 wt % ^{240}Pu)	89.18	–
5	7	Power distribution	529 (265 8 wt % ^{240}Pu) (264 UO_2)	49.90	–
6	8	Power distribution	529 (265 24 wt % ^{240}Pu) (264 UO_2)	89.64	–
7	9	Power distribution	576 (288 24 wt % Pu^{240}) (288 UO_2)	73.42	–
8	10	Power distribution	625 (313 24 wt % ^{240}Pu) (312 UO_2)	63.49	–
9	11	Power distribution	505 (249 24 wt % ^{240}Pu) (256 UO_2)	93.69	–

[a]These are clean experiments that contain no boron.
[b]All experiments were performed in a 1.7526-cm lattice.

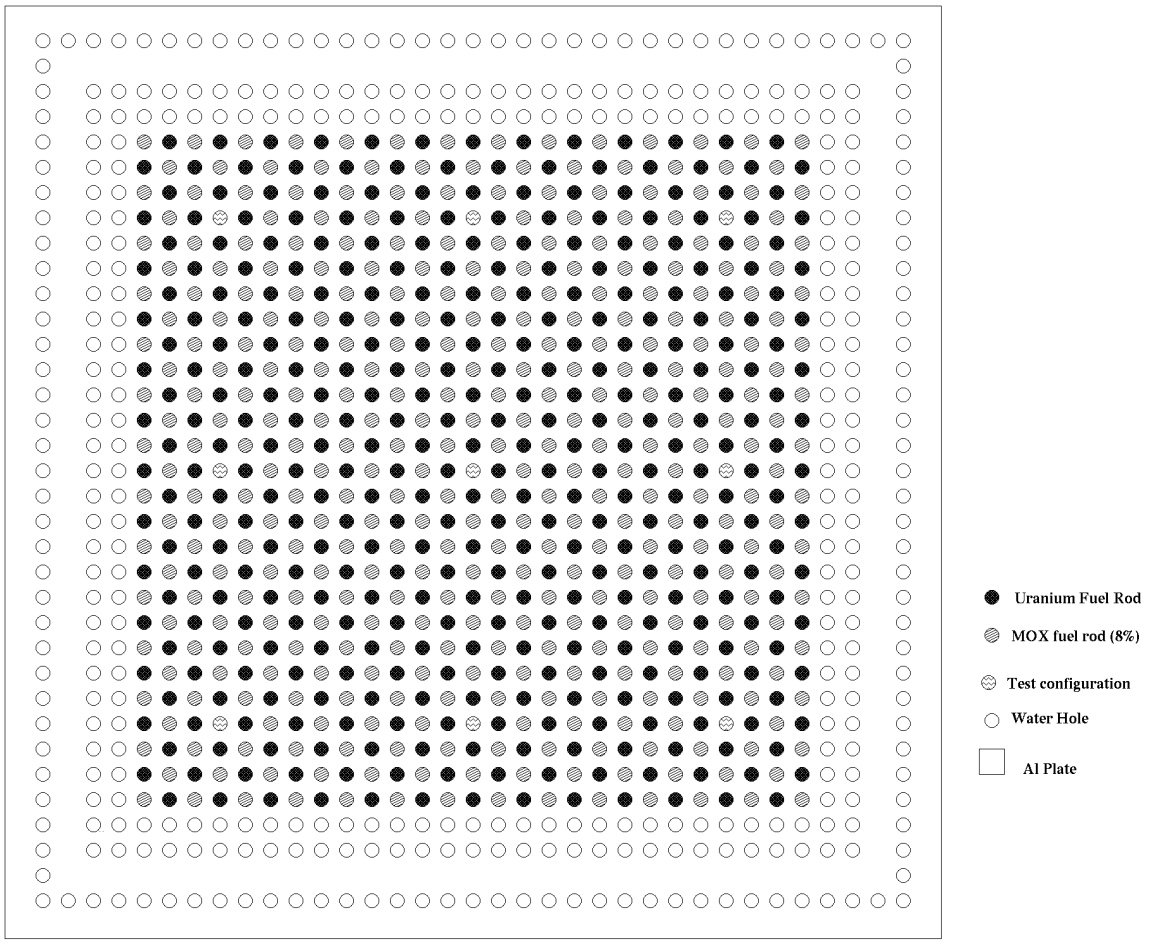

Fig. 5. A 27 × 27 salt-and-pepper core configuration composed of 8 wt % ^{240}Pu and UO_2 with uniformly distributed nine-rod pattern in a 1.7526-cm lattice.

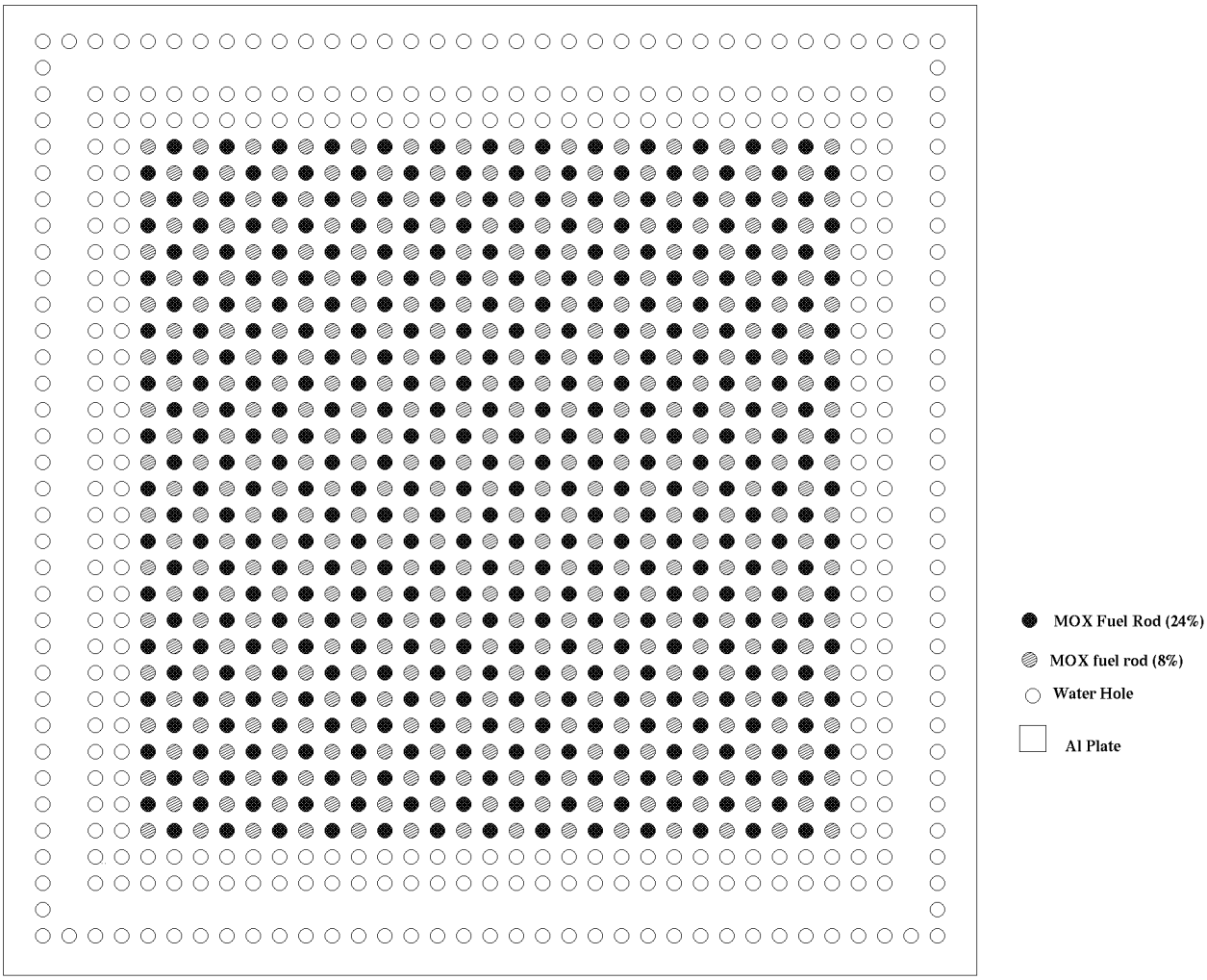

Fig. 6. A 27 × 27 salt-and-pepper core configuration composed of 8 wt % ^{240}Pu and 24 wt % ^{240}Pu fuels.

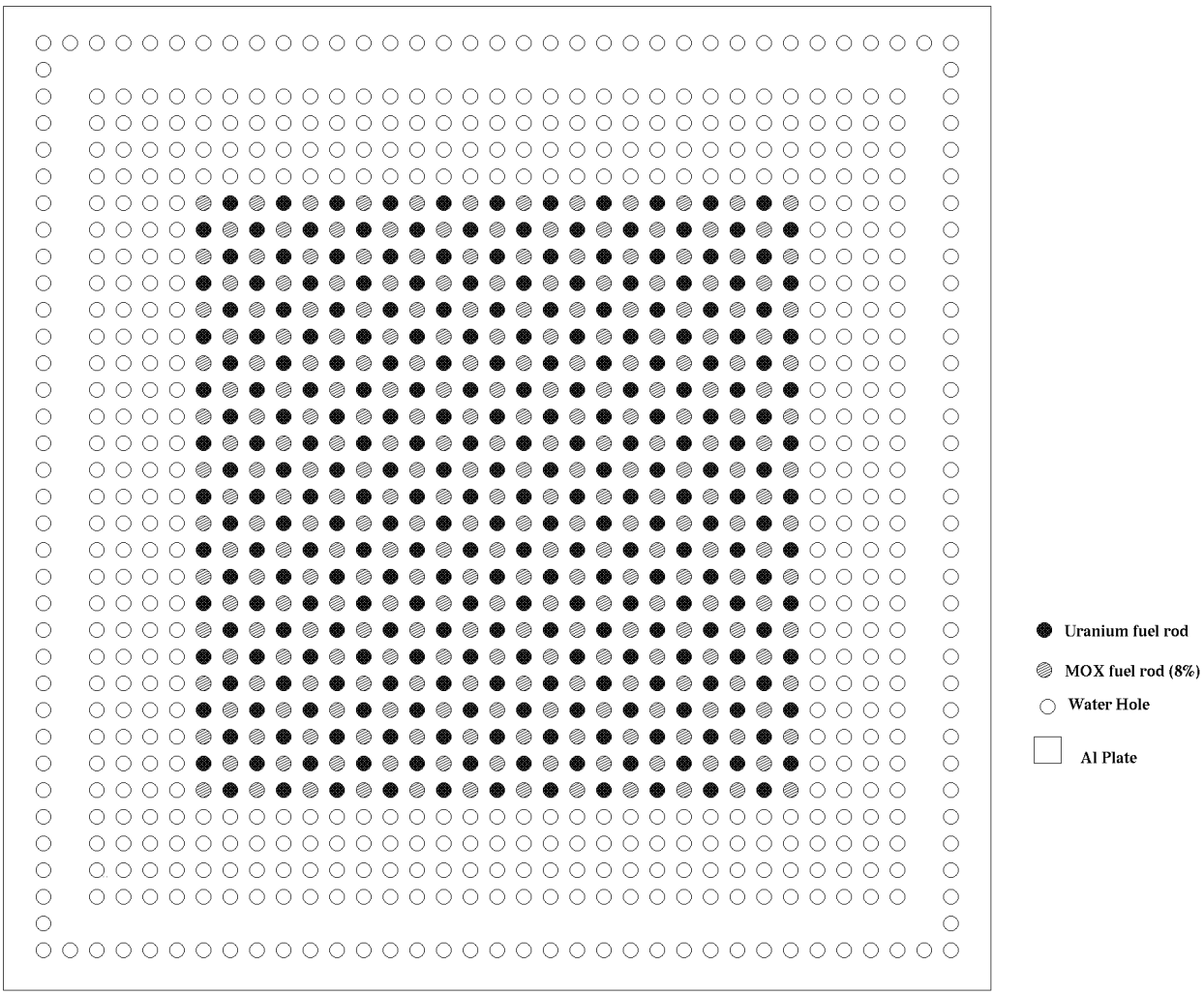

Fig. 7. A 23 × 23 salt-and-pepper core configuration composed of 8 wt % ^{240}Pu and UO_2 fuels.

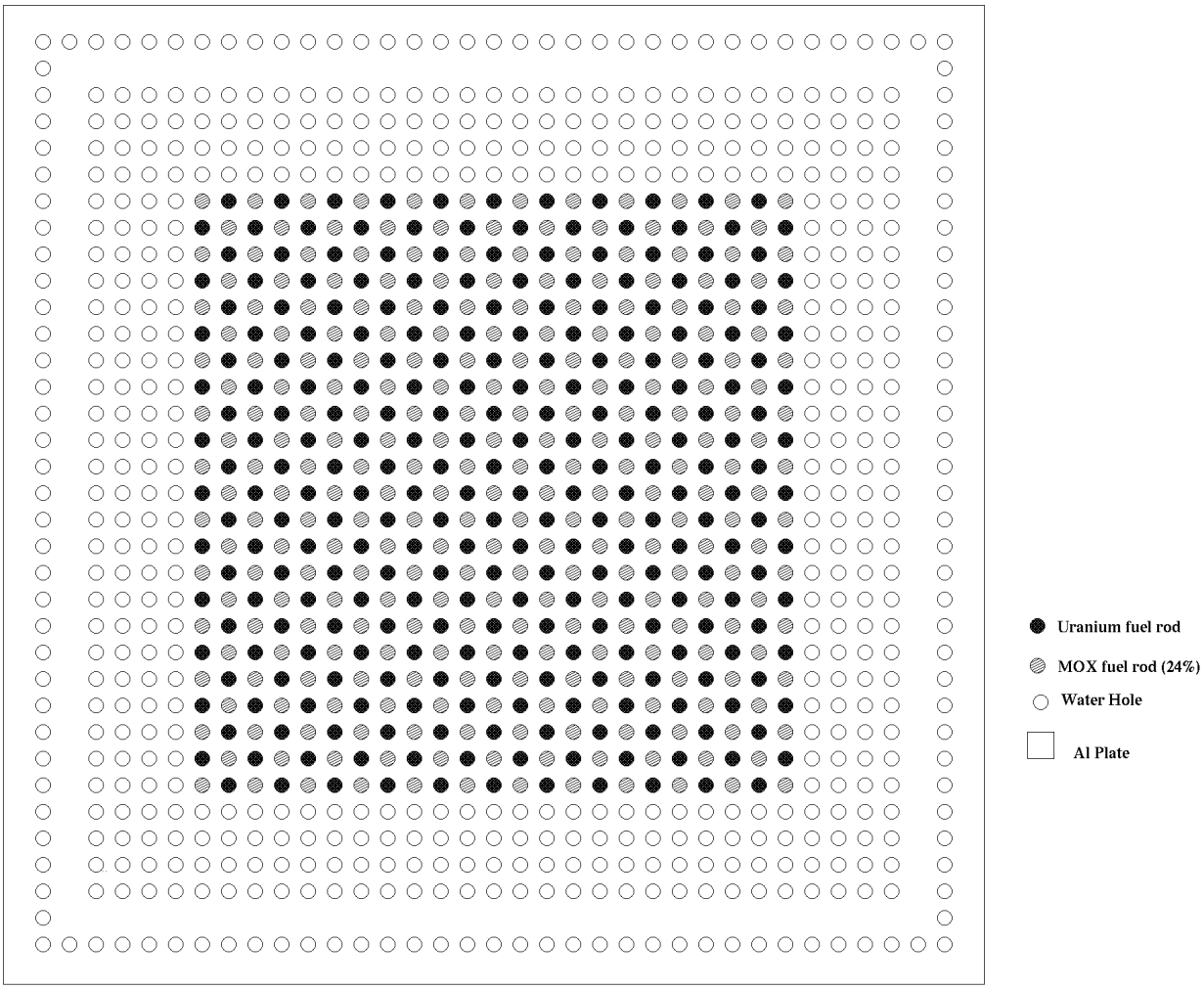

Fig. 8. A 23 × 23 salt-and-pepper core configuration composed of 24 wt % ^{240}Pu and UO_2 fuels.

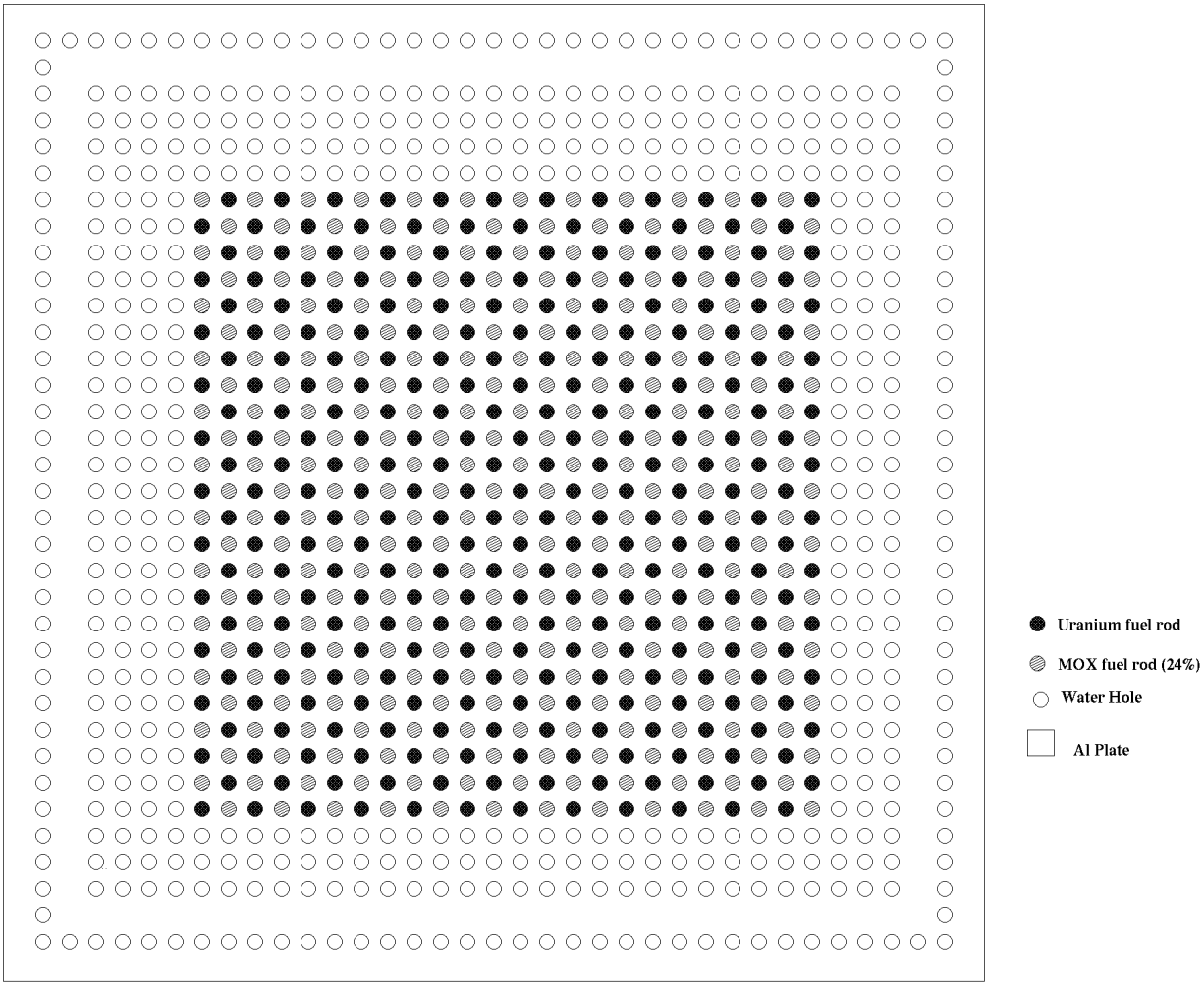

Fig. 9. A 24 × 24 salt-and-pepper core configuration composed of 24 wt % ^{240}Pu and UO_2 fuels.

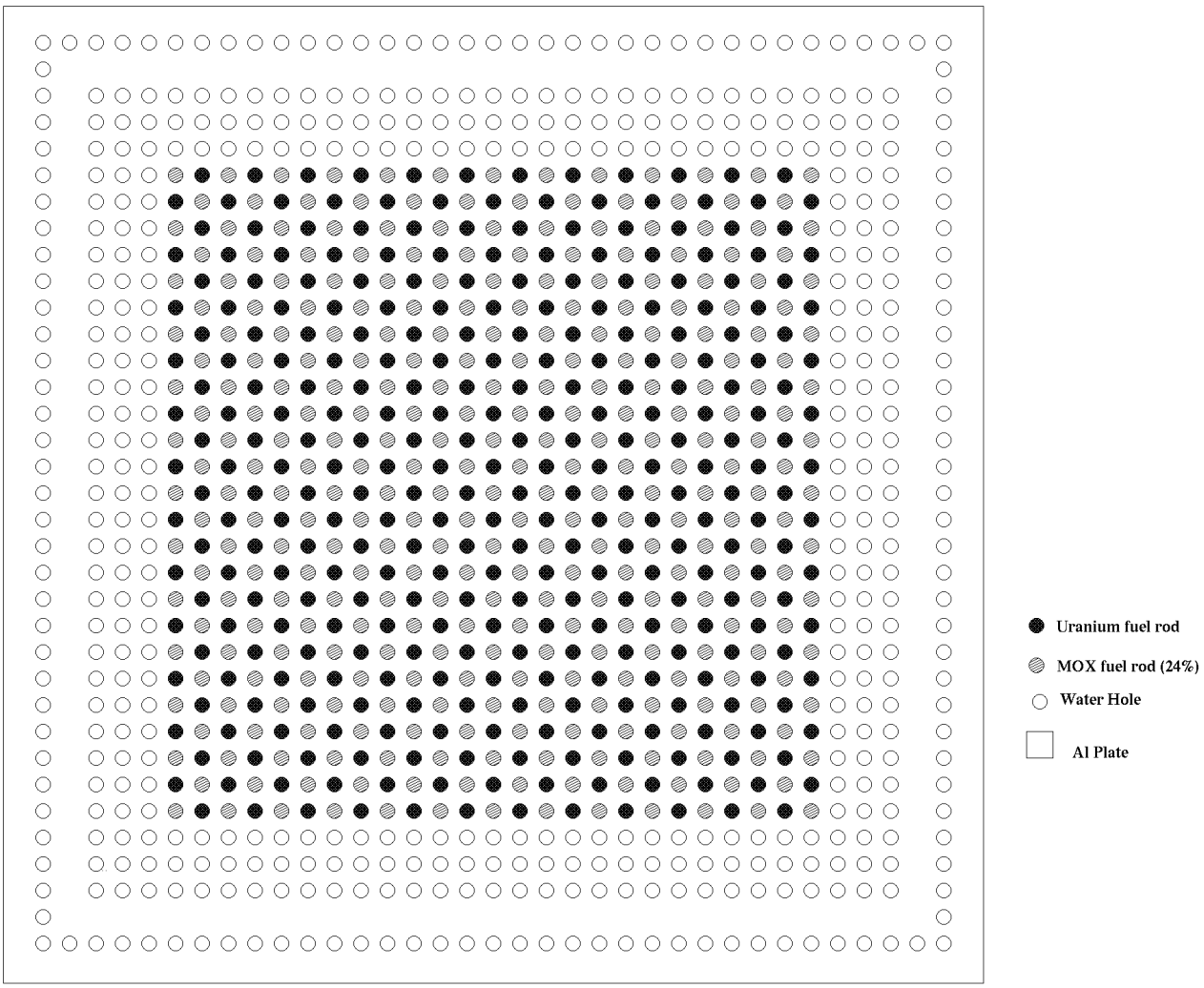

Fig. 10. A 25 × 25 salt-and-pepper core configuration composed of 24 wt % ^{240}Pu and UO_2 fuels.

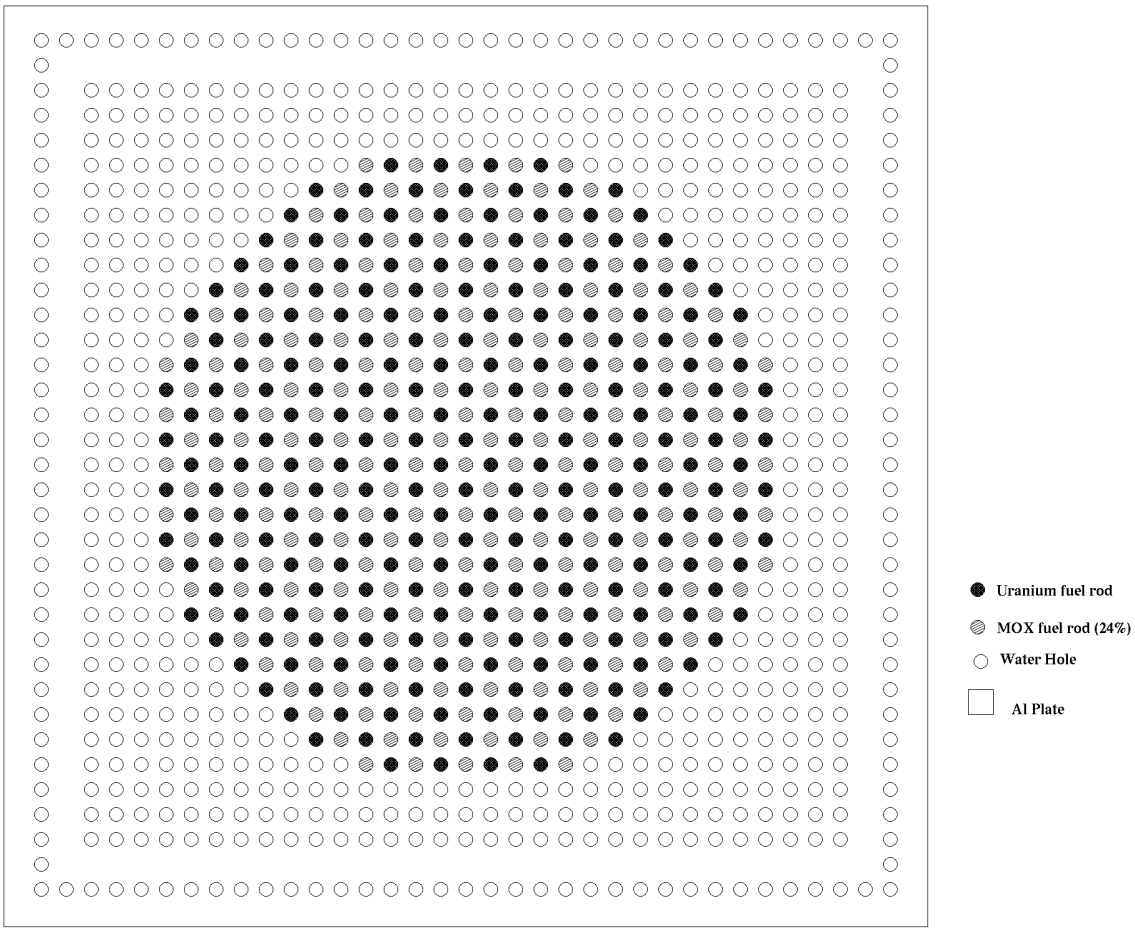

Fig. 11. A cylindrical salt-and-pepper core configuration composed of 24 wt % ^{240}Pu and UO_2 fuels.

1.2.3 Critical Experiments with Concentric-Region Core Configurations

The concentric-region core configurations were constructed by using two different fuels in the inner and outer regions of the core. Various combinations of the available fuels were used during the construction of the core configurations. Eight different core configurations were constructed in this way. Four core configurations were constructed by using 24 wt % ^{240}Pu in the inner region and 8 wt % ^{240}Pu in the outer region. Two of these four experiments were performed for a 1.7526-cm lattice pitch. A third experiment was performed for a 1.9050-cm lattice pitch. Because both types of MOX fuel rods had the same dimensions, the moderator-to-fuel ratio remains the same in these core configurations. However, for one of the configurations with MOX fuel in both the inner and outer regions, the fuel of the outer region was loaded on the diagonal; thus, different moderator-to-fuel volume ratios were introduced in the same configuration for different regions. For this configuration, a 1.9050-cm lattice pitch was used, but the outer region fuel was loaded on the diagonal; therefore, the lattice pitch for the outer region became 2.6942 cm.

In addition to core configurations with MOX fuels, four additional core configurations were constructed by using MOX fuel and UO_2 fuel with different loading combinations. For each of these four configurations, a 1.7526-cm lattice pitch was used. Three core configurations were constructed by using 24 wt % ^{240}Pu and UO_2 fuel with different loading patterns. For two of those cases, UO_2 was loaded in the inner region; for one case, MOX fuel was loaded in the inner region. Moreover, one configuration with an 8 wt % ^{240}Pu inner region and UO_2 outer region was also constructed. The MOX and UO_2 fuel rods have different diameters and heights. In some of the concentric-region core configurations, the MOX and UO_2 fuel rods were used in the same lattice pitch. Therefore for these cases, different moderator-to-fuel volume ratios were obtained in the same configuration.

Installation of the MOX and UO_2 fuels for concentric-region core configurations is given in Fig. 2. For the concentric-region core configurations composed of two different MOX fuels, installation of the core is given in Fig. 1.

Power distribution measurements were made for concentric-region core configurations in clean cores. A photo of a concentric-region core configuration with MOX fuel in the inner region and UO_2 fuel In the outer region is shown in Fig. 12. Reported data for the concentric-region core configurations are listed in Table 2. The related core configurations are presented in Figs. 13–20. For the schematic representation of the core configurations, the cross-section from the aluminum plate is taken as the reference plane. In these figures, the legend label “hole” refers to the fuel rod holes in the aluminum plate. In the absence of fuel or other rods (control rods), these holes were filled with water. Information on core diagram numbers and measurement types are also included in Table 2.

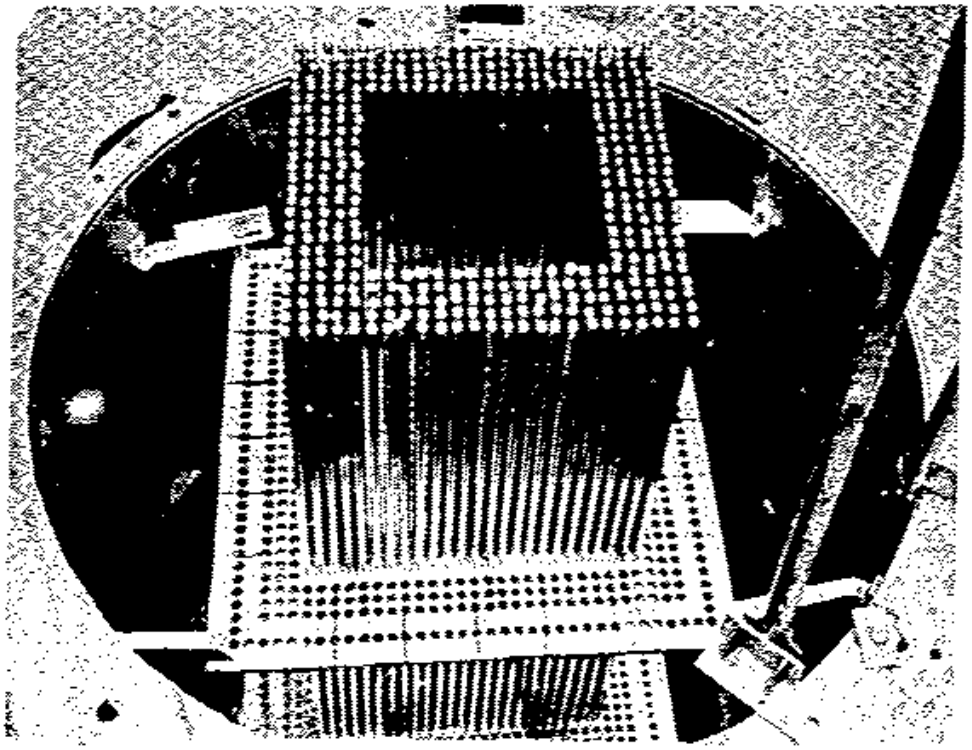

Fig. 12. The concentric-region core configuration with MOX fuel in the inner region and UO_2 fuel in the outer region.

Table 2. Reported data for concentric-region core configurations[a,b]

Case No.	Core diagram (figure number)	Inner region			Outer region			Critical water height (cm)
		Fuel	Number of fuel rods	Lattice pitch (cm)	Fuel	Number of fuel rods	Lattice pitch (cm)	
10	13	8 wt % ^{240}Pu	225	1.7526	UO_2	400	1.7526	50.43
11	14	UO_2	225	1.7526	24 wt %^{240}Pu	400	1.7526	50.08
12	15	24 wt % ^{240}Pu	225	1.7526	UO_2	400	1.7526	79.53
13	16	24 wt % ^{240}Pu	121	1.7526	UO_2	408	1.7526	74.76
14	17	24 wt % ^{240}Pu	225	1.7526	8 wt % ^{240}Pu	492	1.7526	93.48
15	18	24 wt % ^{240}Pu	221	1.7526	8 wt % ^{240}Pu	468	1.7526	95.36
16	19	24 wt % ^{240}Pu	157	1.9050	8 wt % ^{240}Pu	264	1.9050	92.65
17	20	24 wt % ^{240}Pu	89	1.9050	8 wt % ^{240}Pu	143	2.6942	93.42

[a]Power distribution measurements were performed for this type of core configuration.
[b]These are clean core experiments that contain no boron.

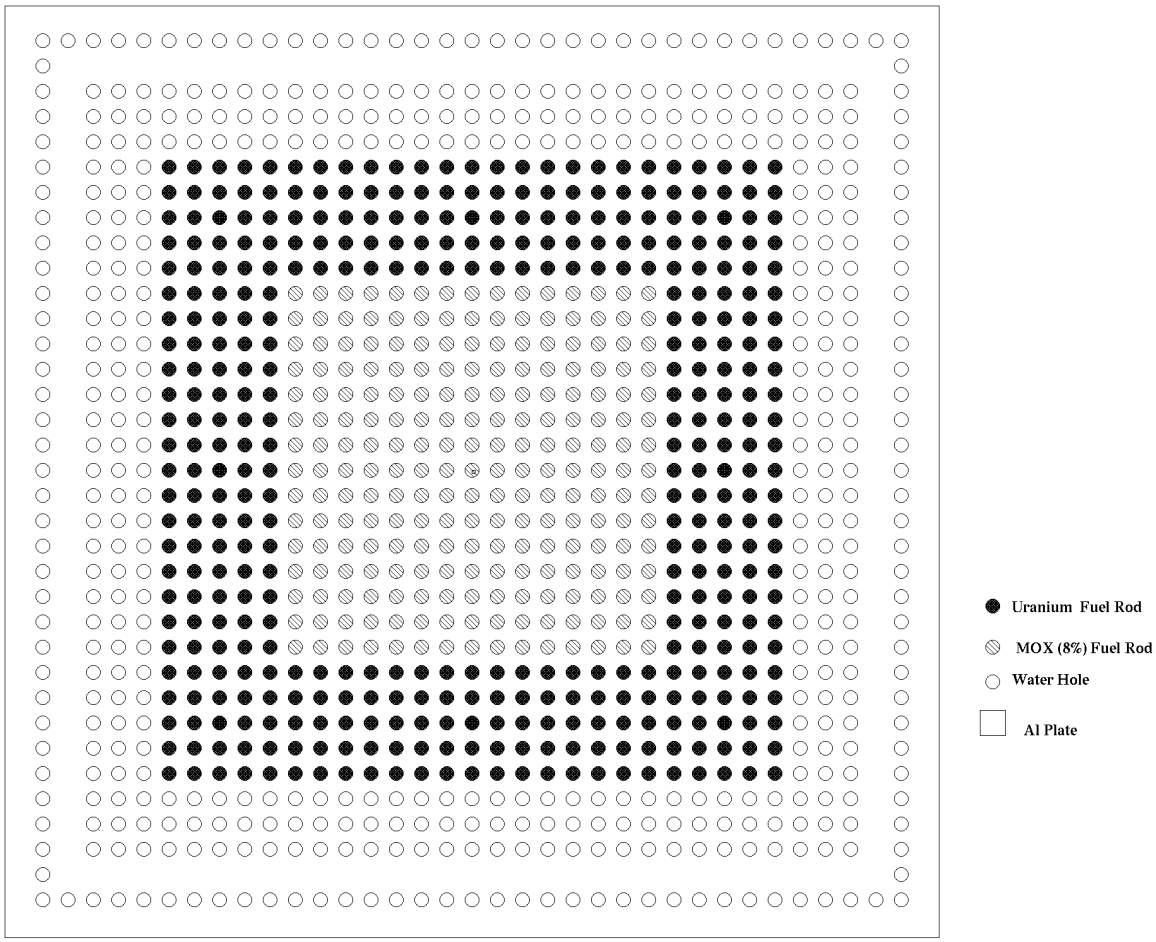

Fig. 13. A 25 × 25 concentric-region core configuration containing a 15 × 15, 8 wt % ^{240}Pu, inner region and UO_2 outer region.

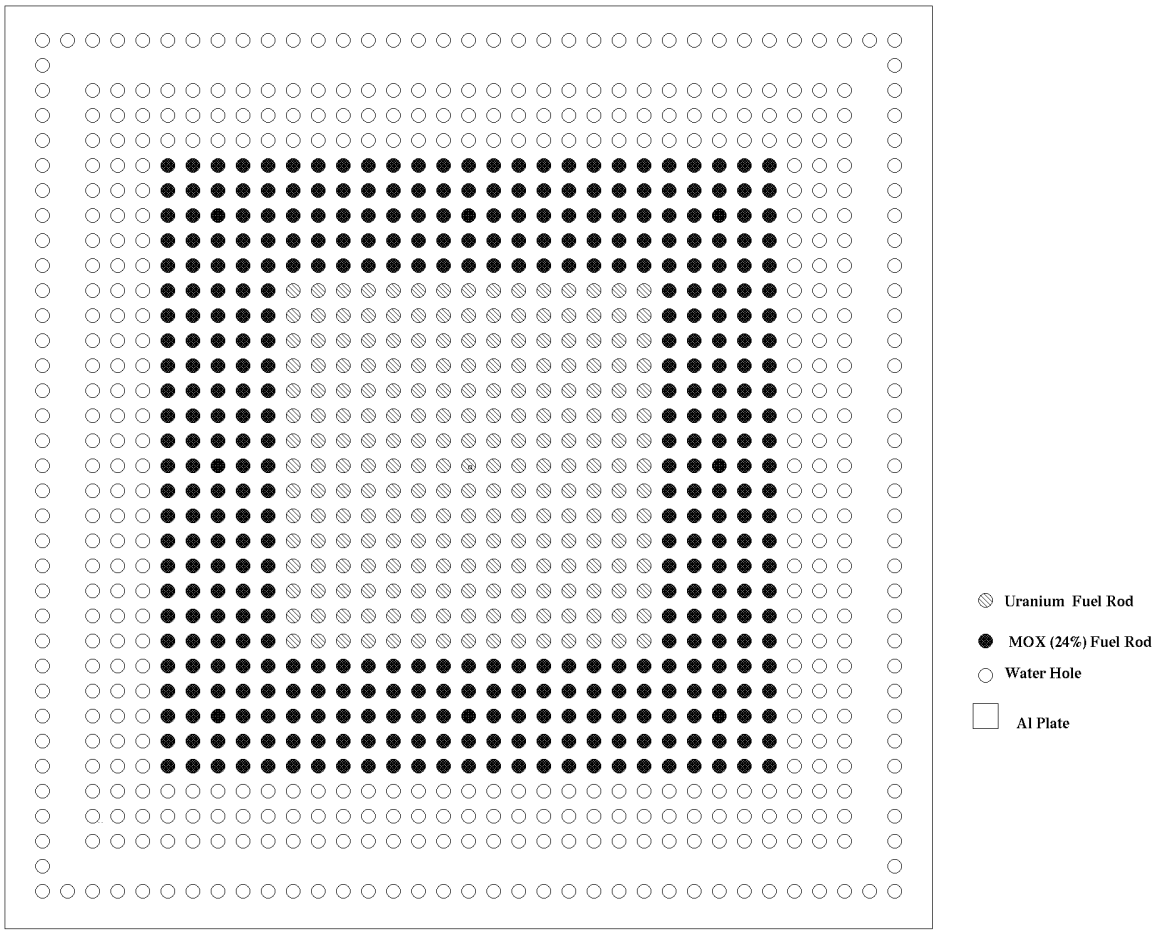

Fig. 14. A 25 × 25 concentric-region core configuration containing a 15 × 15, UO_2 inner region and 24 wt % ^{240}Pu outer region.

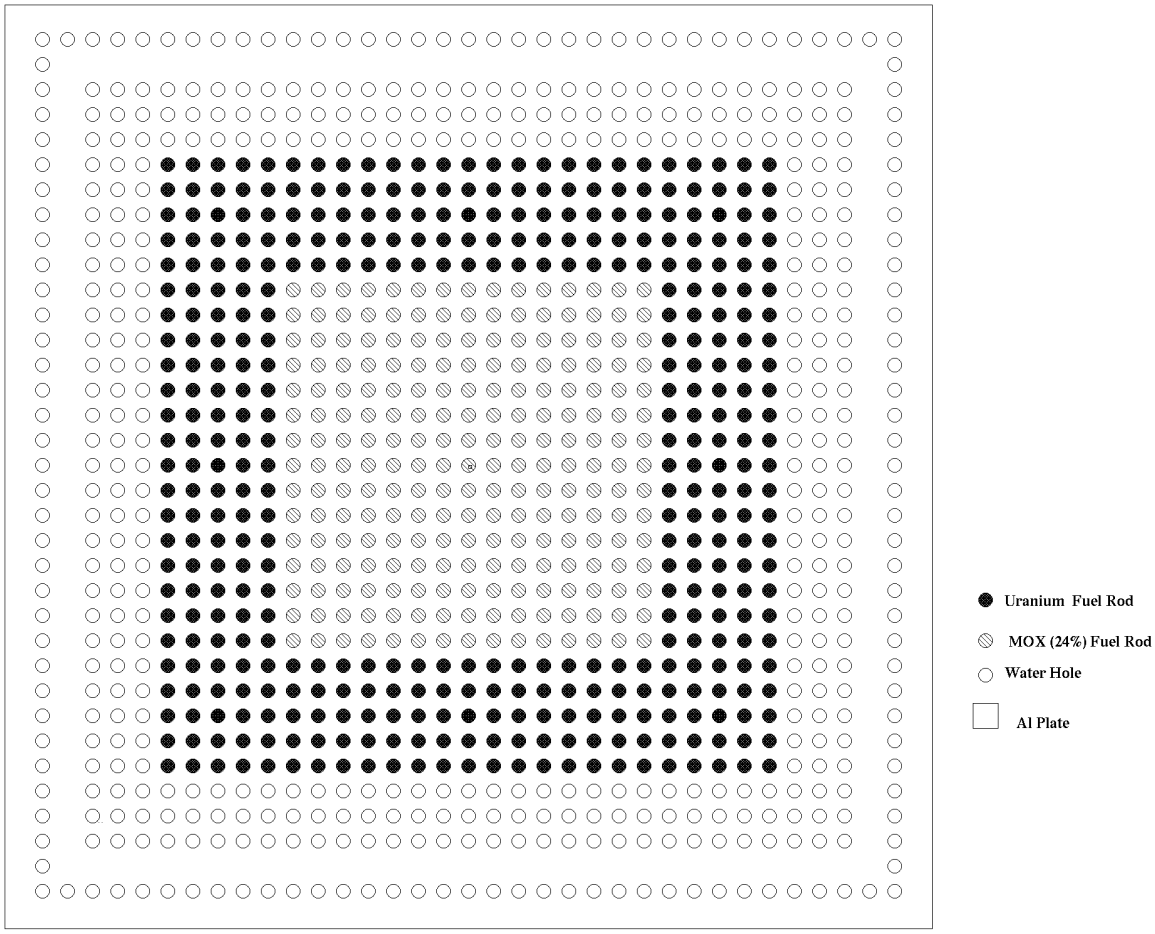

Fig. 15. A 25 × 25 concentric-region core configuration containing a 15 × 15, 24 wt % ^{240}Pu, inner region and UO_2 outer region.

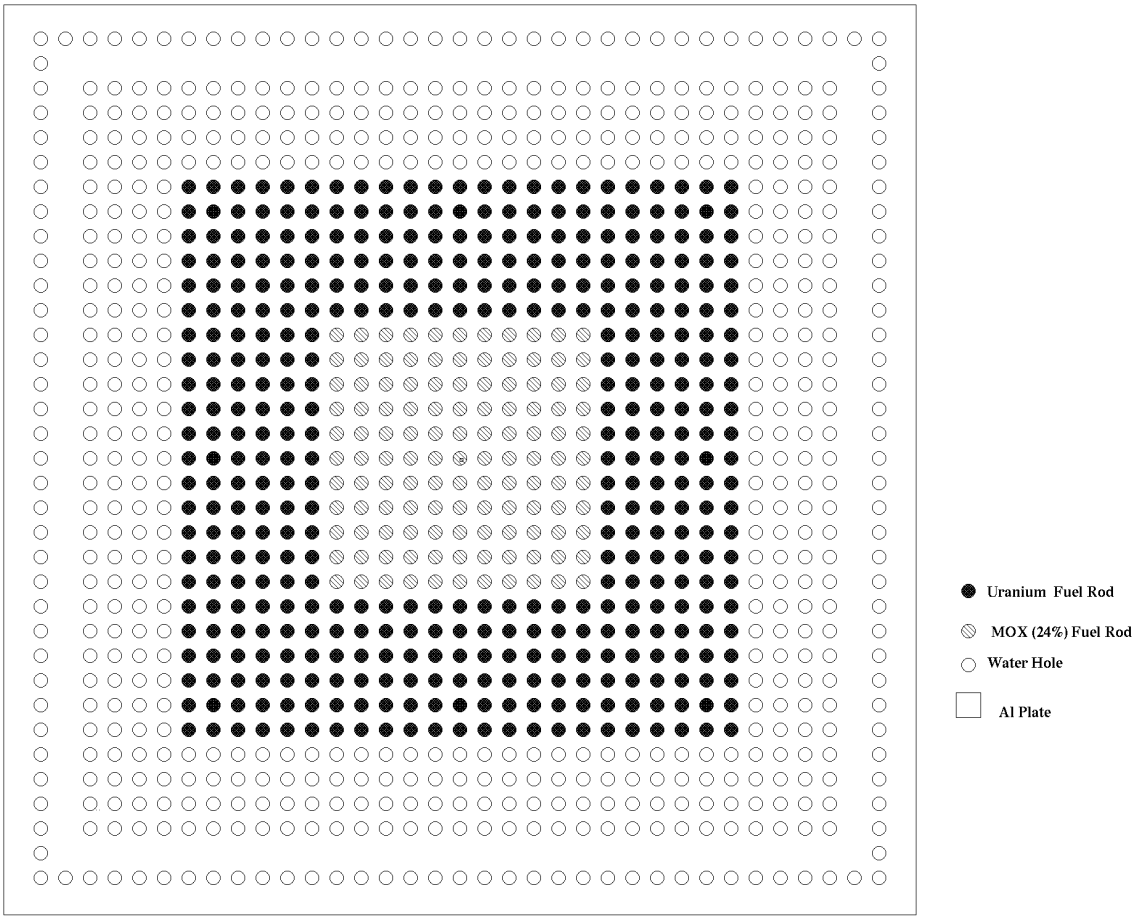

Fig. 16. A 23 × 23 concentric-region core configuration containing an 11 × 11, 24 wt % ^{240}Pu, inner region and UO_2 outer region.

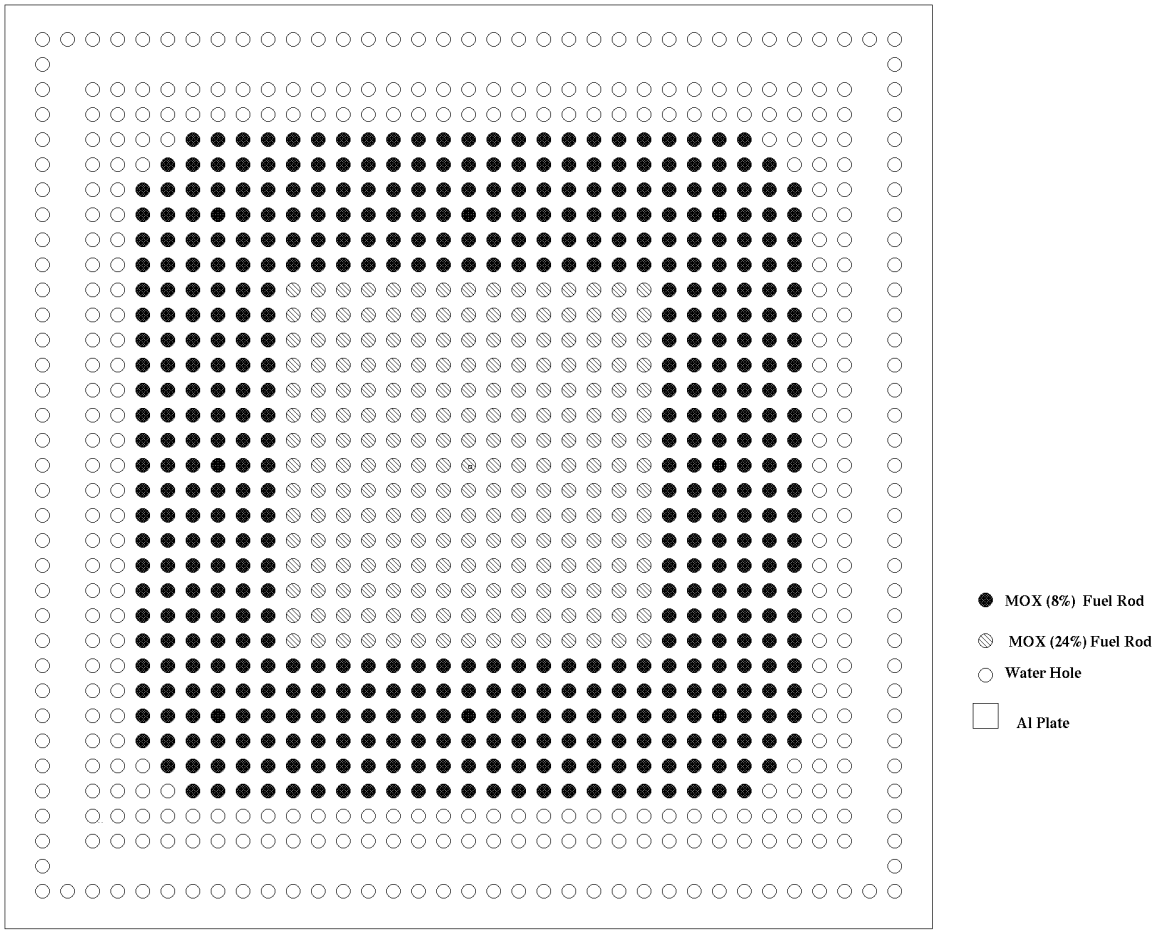

Fig. 17. A 27 × 27 concentric-region core configuration containing a 15 × 15, 24 wt % ^{240}Pu, inner region and 8 wt % ^{240}Pu outer region.

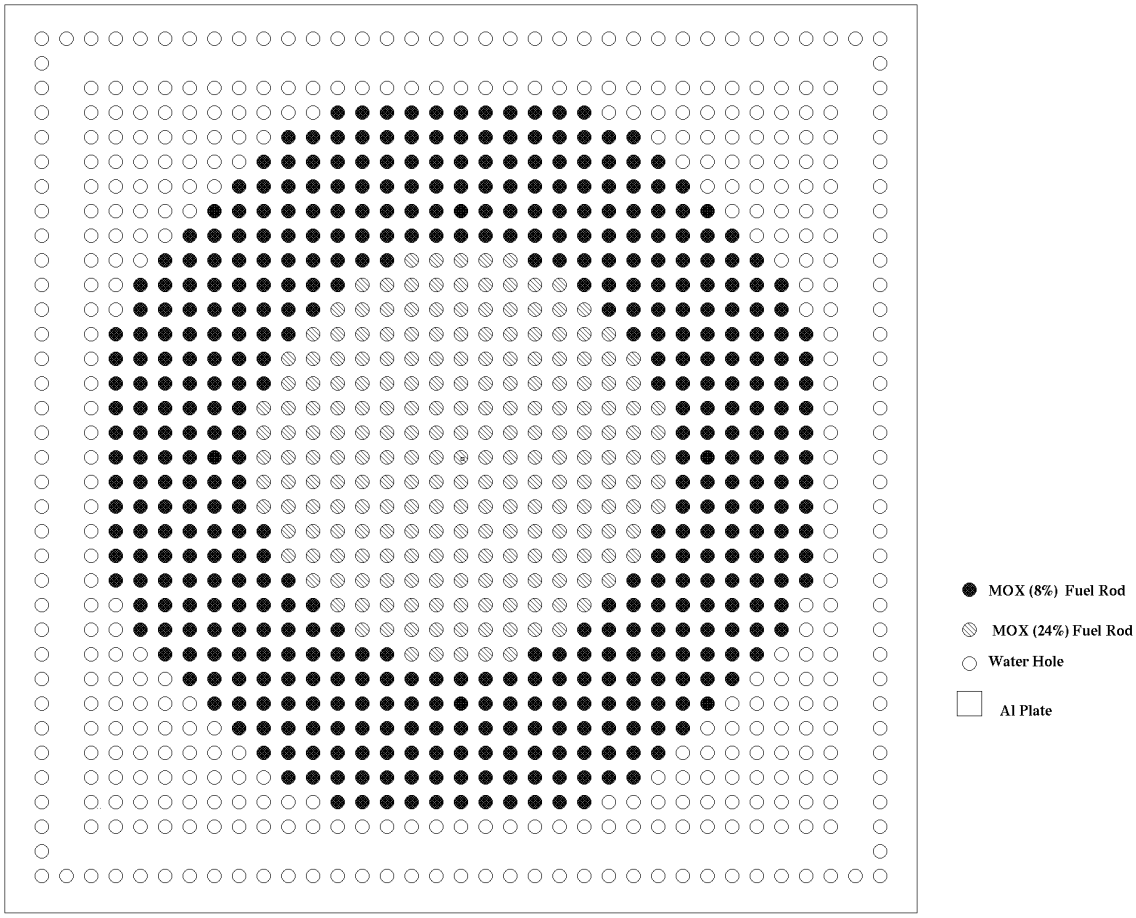

Fig. 18. A cylindrical concentric-region core configuration containing a 24 wt % ^{240}Pu inner region and an 8 wt % ^{240}Pu outer region.

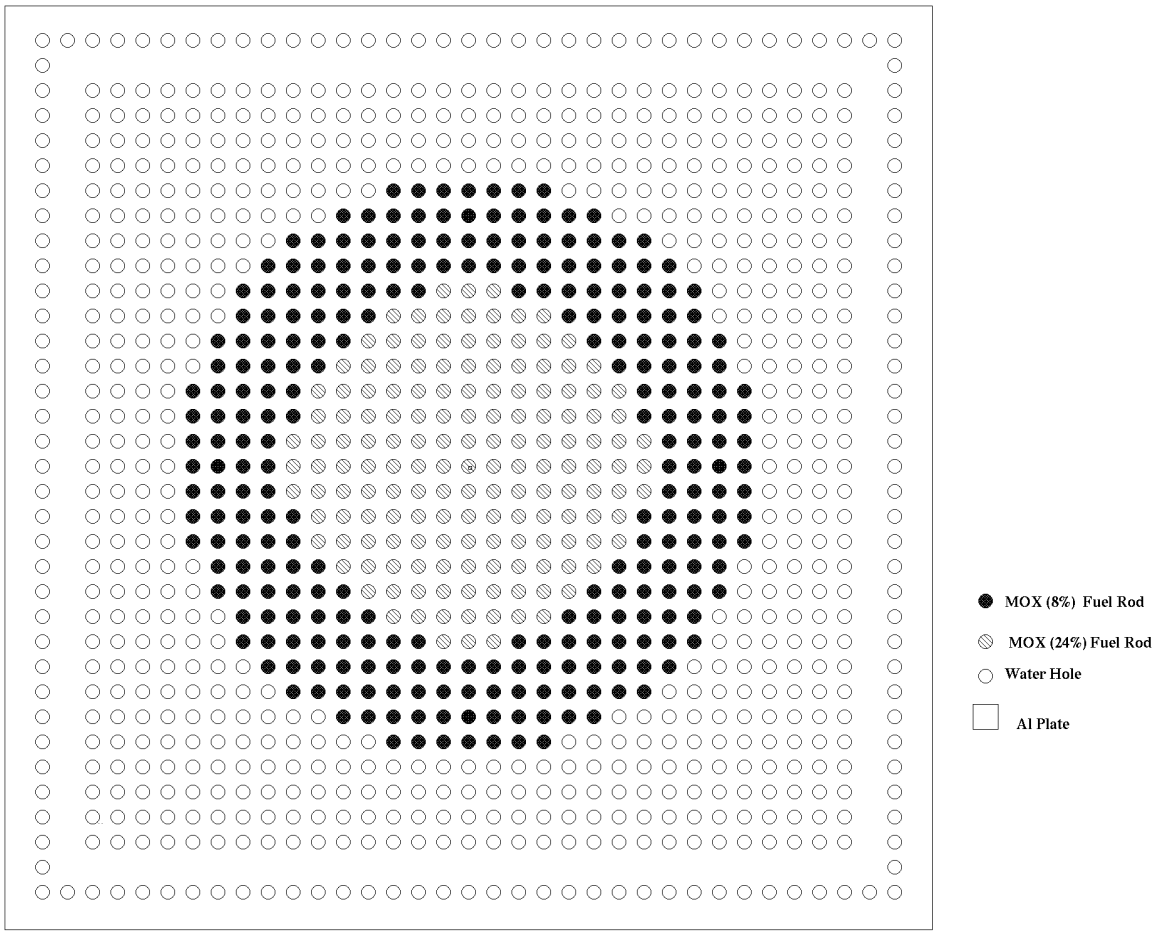

Fig. 19. A cylindrical concentric-region core configuration containing a 24 wt % ^{240}Pu inner region and an 8 wt % ^{240}Pu outer region.

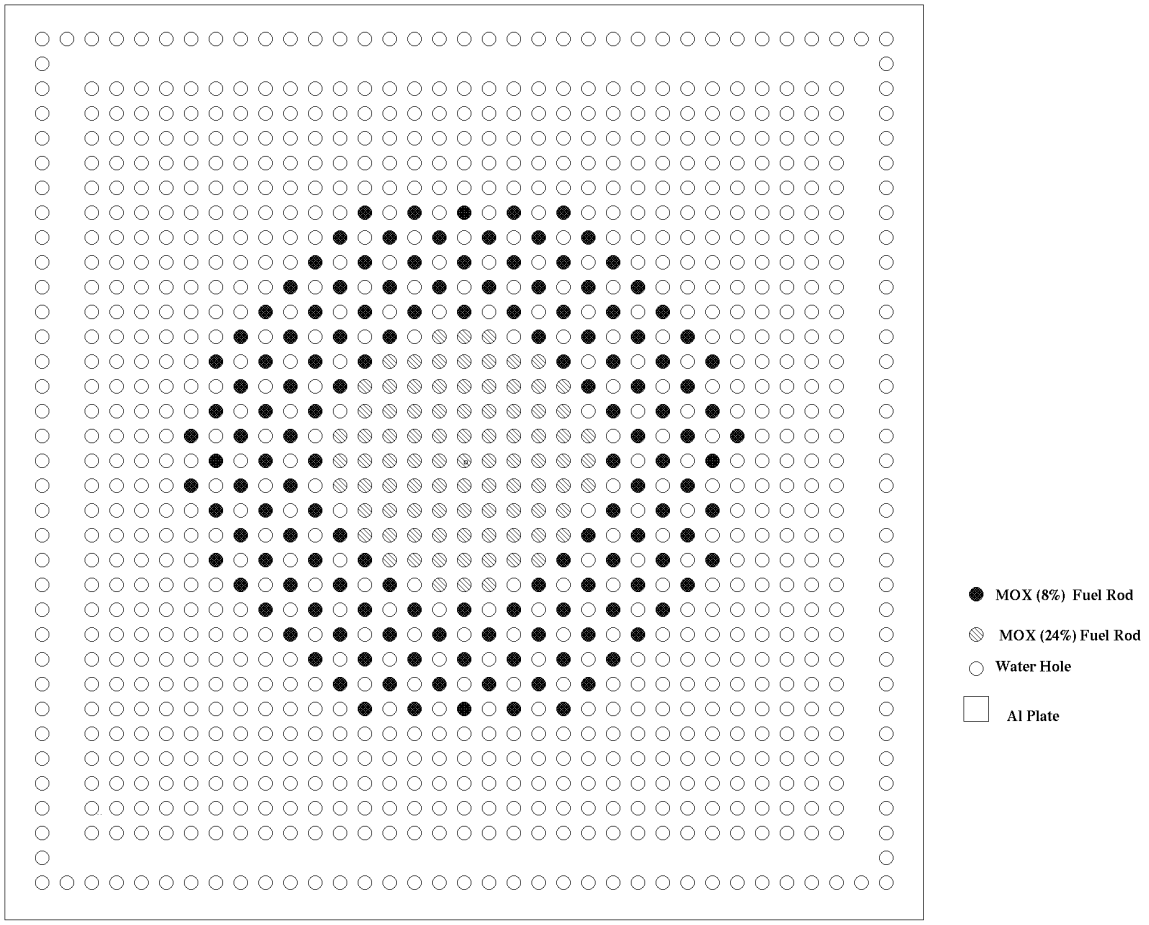

Fig. 20. A cylindrical concentric-region core configuration containing a 24 wt % ^{240}Pu inner region and an 8 wt % ^{240}Pu outer region with a regional variation in lattice pitch.

1.2.4 Critical Experiments with Multiregion Slab Core Configurations

The multiregion core configurations can be described as two rectangular slabs loaded with UO_2, sandwiching a center region loaded with MOX fuel. Because the MOX and UO_2 fuel rods have different diameters, two different lattice pitches were used for this multiregion core configuration. In the UO_2 regions, a smaller lattice pitch was used compared to the MOX (central) region to maintain the same moderator-to-fuel ratio throughout the core. The lattice pitch for UO_2 slabs was 1.4605 cm (0.575 in.), whereas the lattice pitch for MOX fuel was 1.7526 cm (0.69 in.). In this way, the moderator-to-fuel ratio was the same for both the MOX and UO_2 regions. A water gap of 1.608-cm (0.633-in.) was present between the slab regions. This gap was between the unit cells; therefore, the distance between the centers of the MOX and UO_2 fuel rods is 3.21455 cm (1.608-cm plus one-half of the MOX and UO_2 lattice pitches).

The reactivity worths of local voids were measured in both clean and borated multiregion cores. Local voids were simulated by inserting aluminum tubes between the fuel rods to the center of the lattice. Power distribution measurements were made in a number of different multiregion slab configurations for both clean and borated cores. Two additional core configurations were constructed, and all available types of fuels were used in these configurations. One of those core configurations was constructed by using the 24 wt % ^{240}Pu fuel in the inner region and the 8 wt % ^{240}Pu fuel in the outer region. The other multiregion core configuration contains alternate rows of 8 wt % and 24 wt % ^{240}Pu fuels in the central region.

Installation of the MOX and UO_2 fuel rods in a multiregion slab core configuration was shown in Fig. 3. Layouts of the MOX and UO_2 fuel in a multiregion core configurations are shown in different ways in Figs. 21–24.

Reported data for multiregion core configurations are given in Table 3. The experimental core configurations are given in Figs. 25–31.

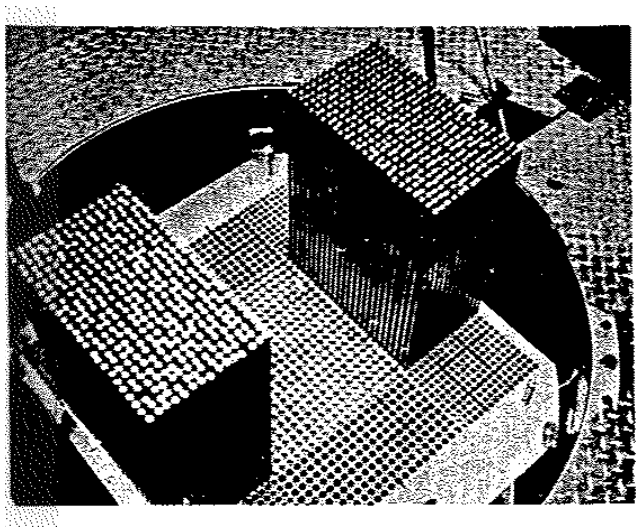

Fig. 21. Multiregion core configuration with the UO_2 slabs sandwiching MOX in central region.

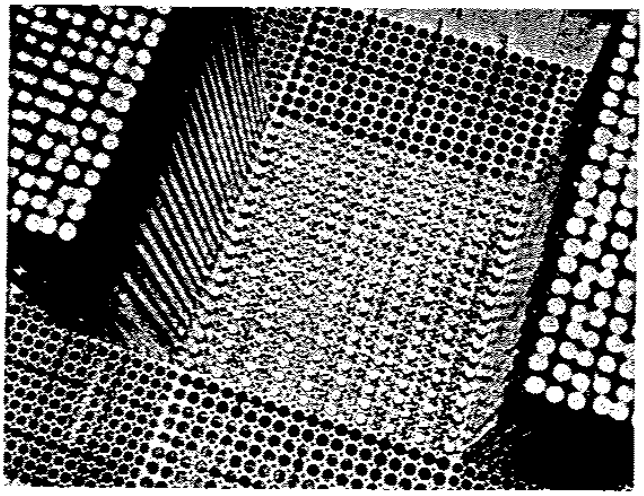

Fig. 22. Multiregion core configuration with alternating rows of 8 wt % and 24 wt % ^{240}Pu MOX in the central region and UO_2 fuel in the outer regions.

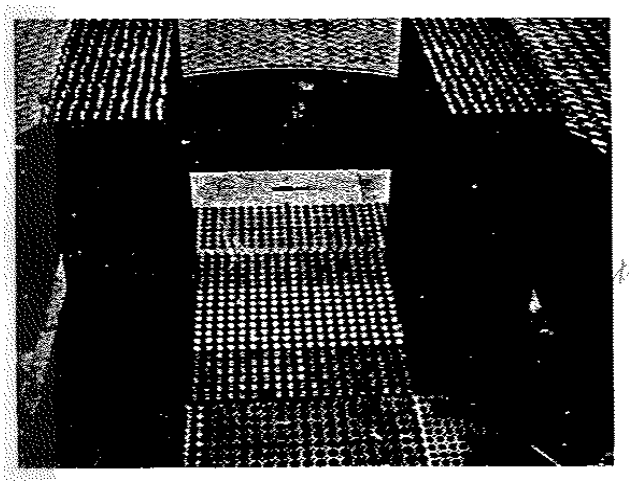

Fig. 23. A multiregion core configuration with traverse slabs of 8 wt % ^{240}Pu and 24 wt % ^{240}Pu MOX in the central region and UO_2 fuel in the outer regions.

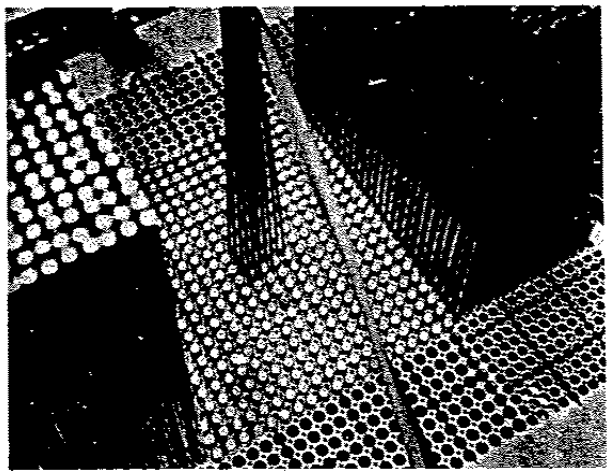

Fig. 24. A multiregion core configuration with a 4 × 4 local void simulation using aluminum tubes.

Table 3. Reported data for multiregion slab core configurations[a]

Case No	Core diagram (figure number)	Measurement type	Number of UO_2 fuel rods	Number of MOX fuel rods[b]	Boron concentration	Critical water height (cm)	Test configuration
18	–	Reactivity	460	361	0	62.83	Reference core
19	25	Reactivity	460	361	0	64.45	4 × 4 void tubes
20	26	Reactivity	460	361	0	72.74	10 × 10 aluminum void tubes
21	27	Reactivity	810	437	0	39.35	Reference core
22	28	Reactivity	810	437	0	41.65	10 × 10 aluminum void tubes
23	–	Reactivity	810	437	0	47.04	16 × 22 aluminum void tubes
24	27	Reactivity	810	437	526	69.07	Reference core
25	29	Reactivity	810	437	526	70.36	4 × 4 aluminum void tubes
26	28	Reactivity	810	437	526	77.70	10 × 10 aluminum void tubes
27	–	Reactivity	810	437	526	81.75	12 × 12 aluminum void tubes
28	–	Power distribution	460	361	0	62.83	Reference core
29	25	Power distribution	460	361	0	64.45	4 × 4 aluminum void tubes
30	26	Power distribution	460	361	0	72.74	10 × 10 aluminum void tubes
31	27	Power distribution	810	437	526	69.04	Reference core
32	29	Power distribution	810	437	526	70.31	4 × 4 aluminum void tubes
33	28	Power distribution	810	437	526	77.73	10 × 10 aluminum void tubes
34	30	Power distribution	500	228 (8 wt % ^{240}Pu) 171 (24 wt % ^{240}Pu)	0	75.41	–
35	31	Power distribution	500	210 (8 wt % ^{240}Pu) 189 (24 wt % ^{240}Pu)	0	71.05	–

[a]Lattice pitch for the UO_2 slab was 1.4605 cm and 1.7526 cm for the MOX region for all configurations.
[b]MOX fuel refers to 8 wt % ^{240}Pu fuel if any specific information is not provided.

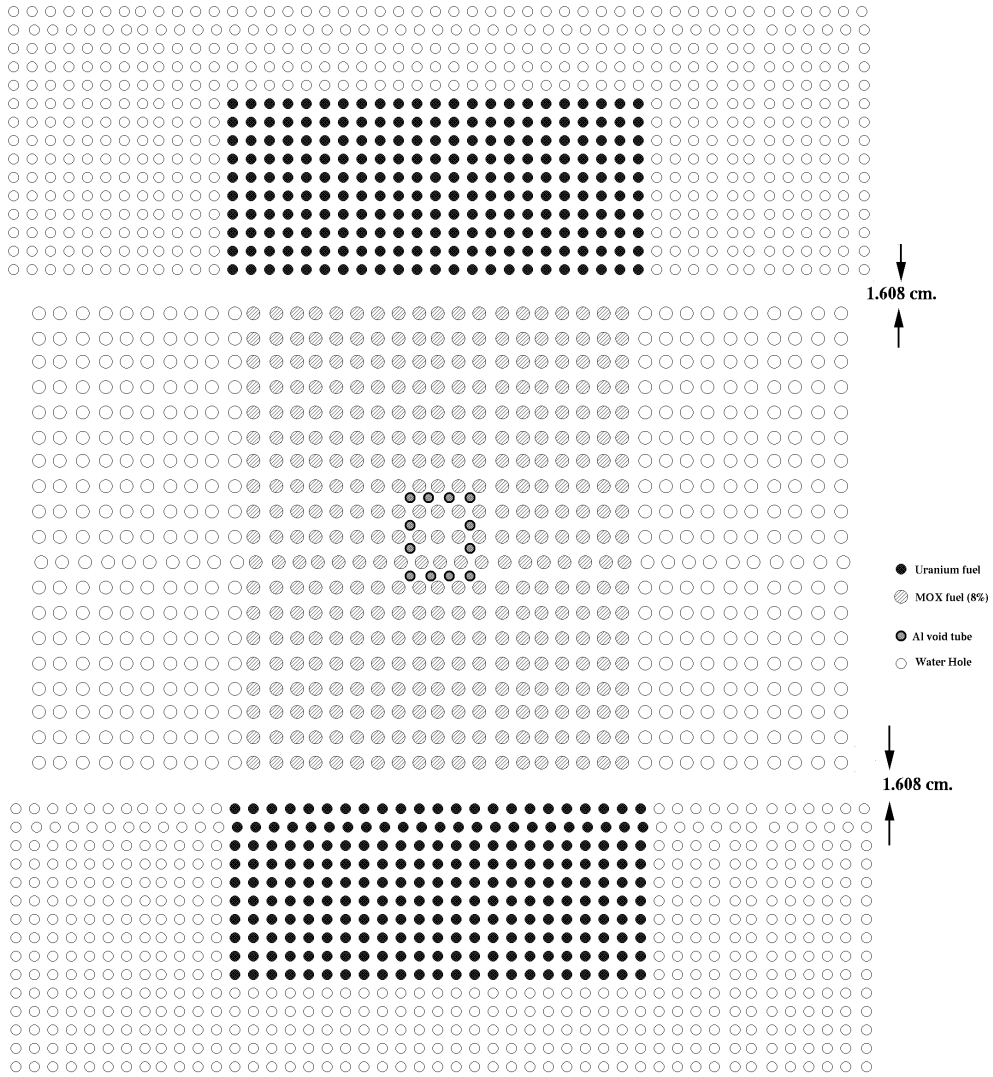

Fig. 25. The multiregion slab core configuration containing an 8 wt % ^{240}Pu central region (19 × 19) and UO_2 outer regions (10 × 23) with a 4 × 4 central void pattern.

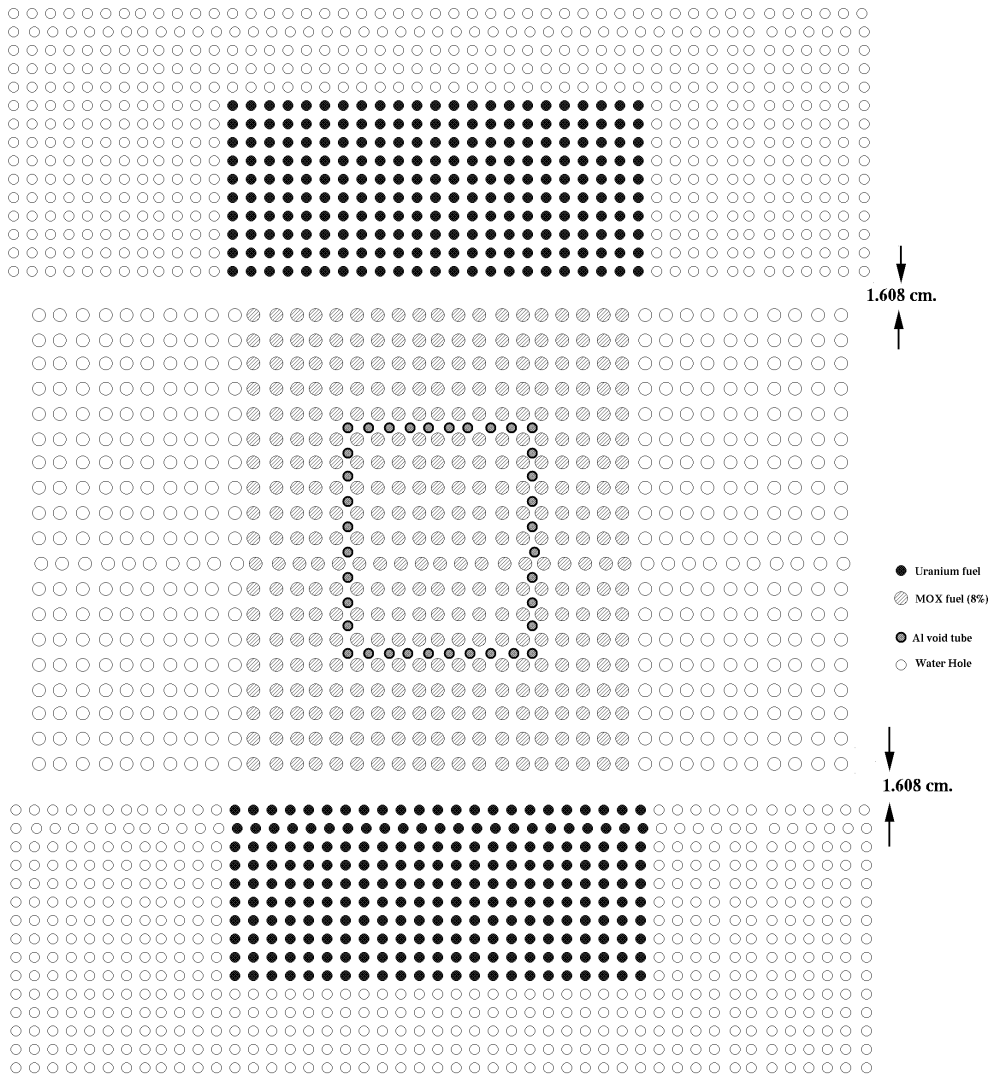

Fig. 26. A multiregion slab core configuration containing an 8 wt % ^{240}Pu central region (19×19) and UO_2 outer regions (10×23) with a 10×10 central void pattern.

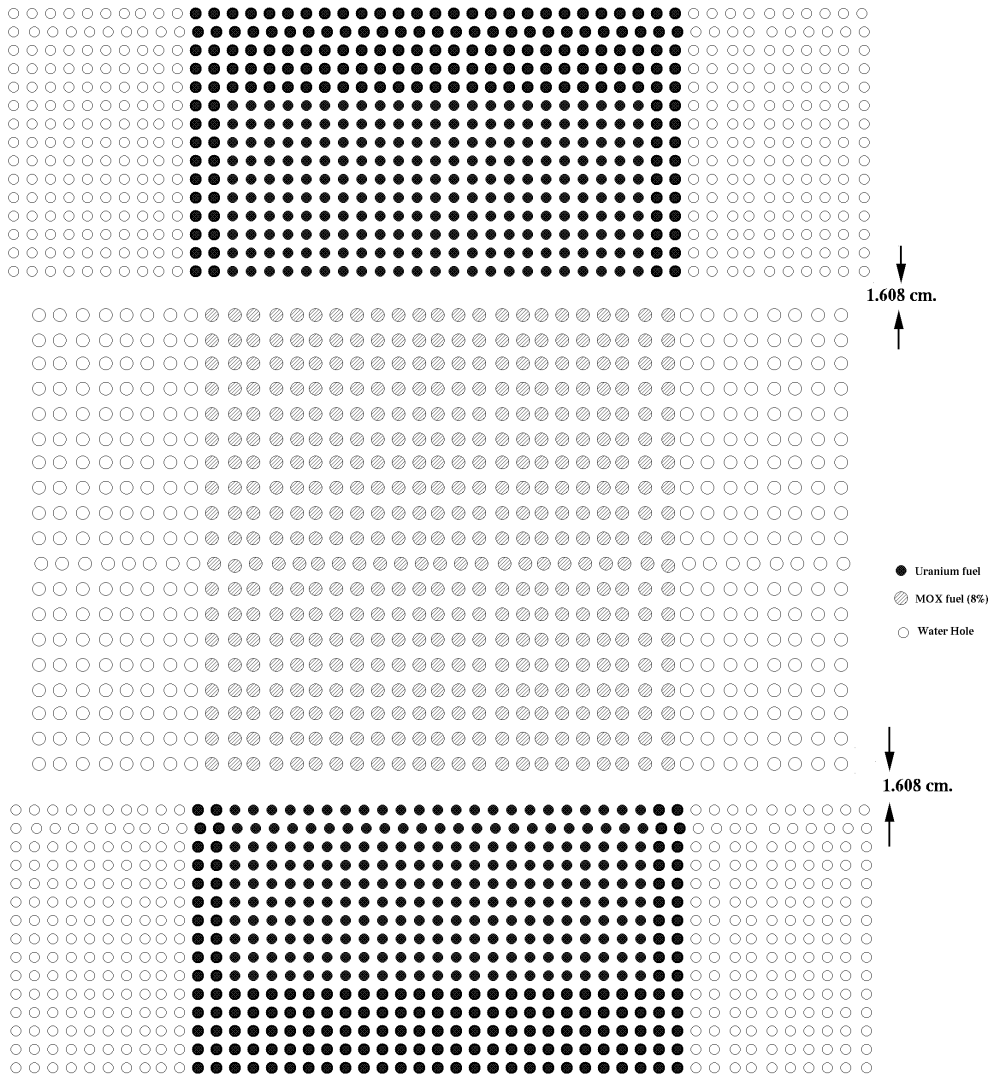

Fig. 27. A multiregion slab reference core configuration containing an 8 wt % ^{240}Pu central region (19 × 23) and UO_2 outer regions (15 × 27).

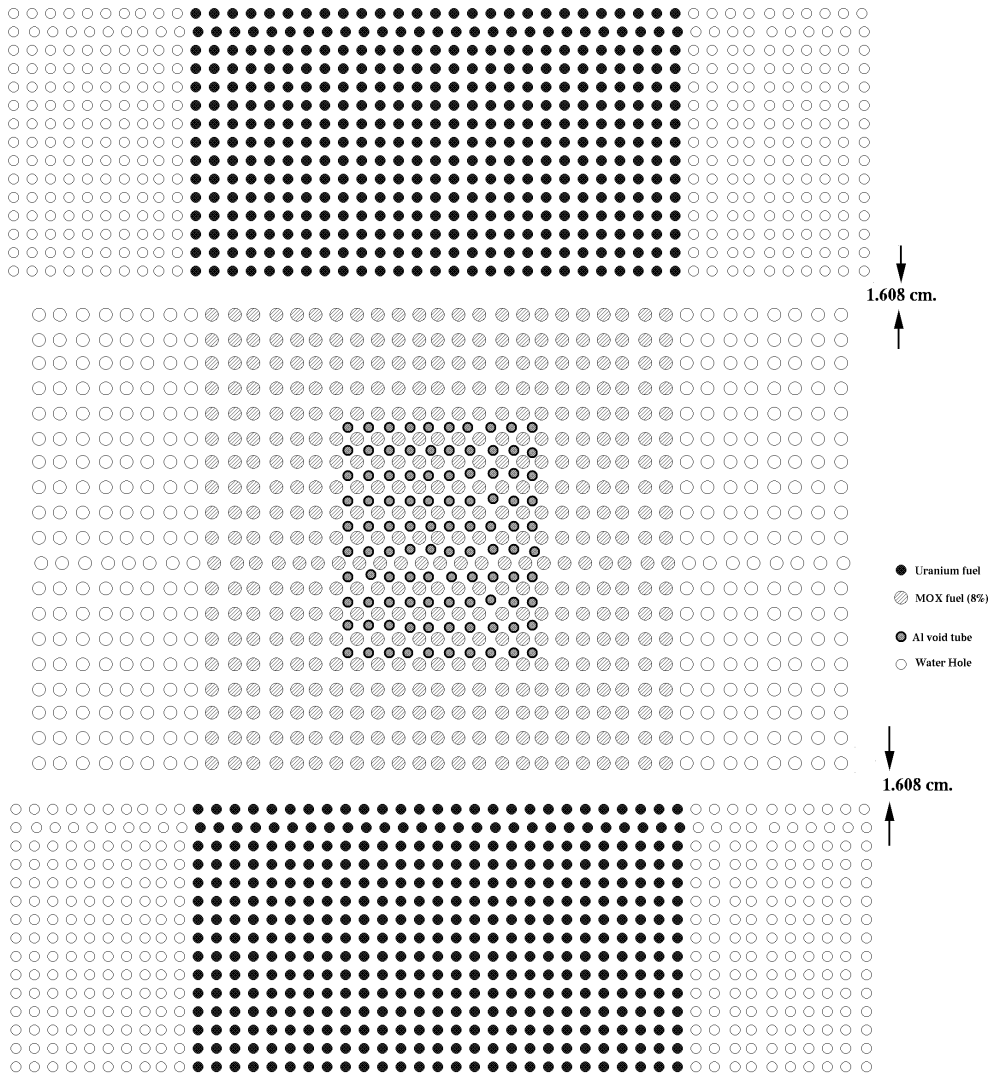

Fig. 28. A multiregion slab core configuration containing an 8 wt % ^{240}Pu central region (19 × 23) and UO_2 outer regions (15 × 27) with a 10 × 10 central void pattern.

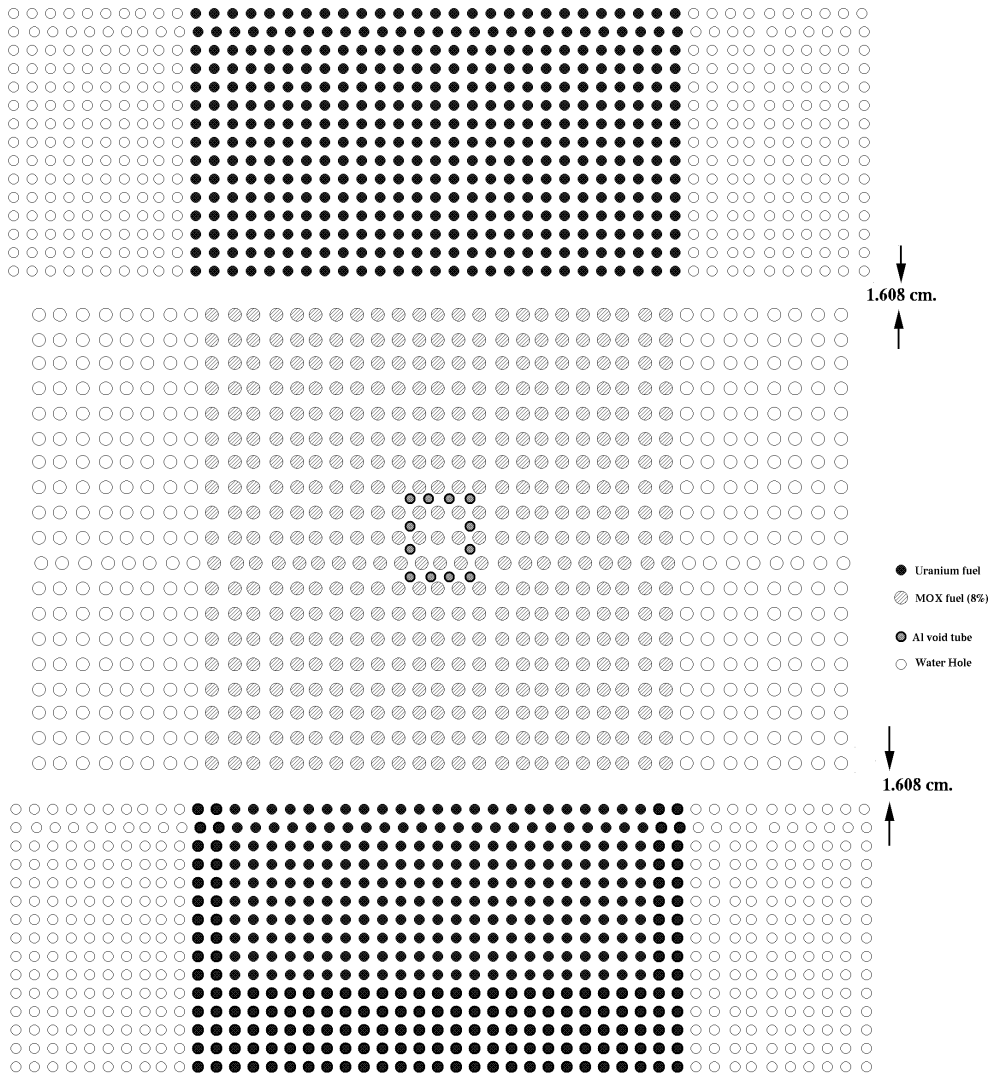

Fig. 29. A multiregion slab core configuration containing an 8 wt % ^{240}Pu central region (19 × 23) and UO_2 outer regions (15 × 27) with a 4 × 4 central void pattern.

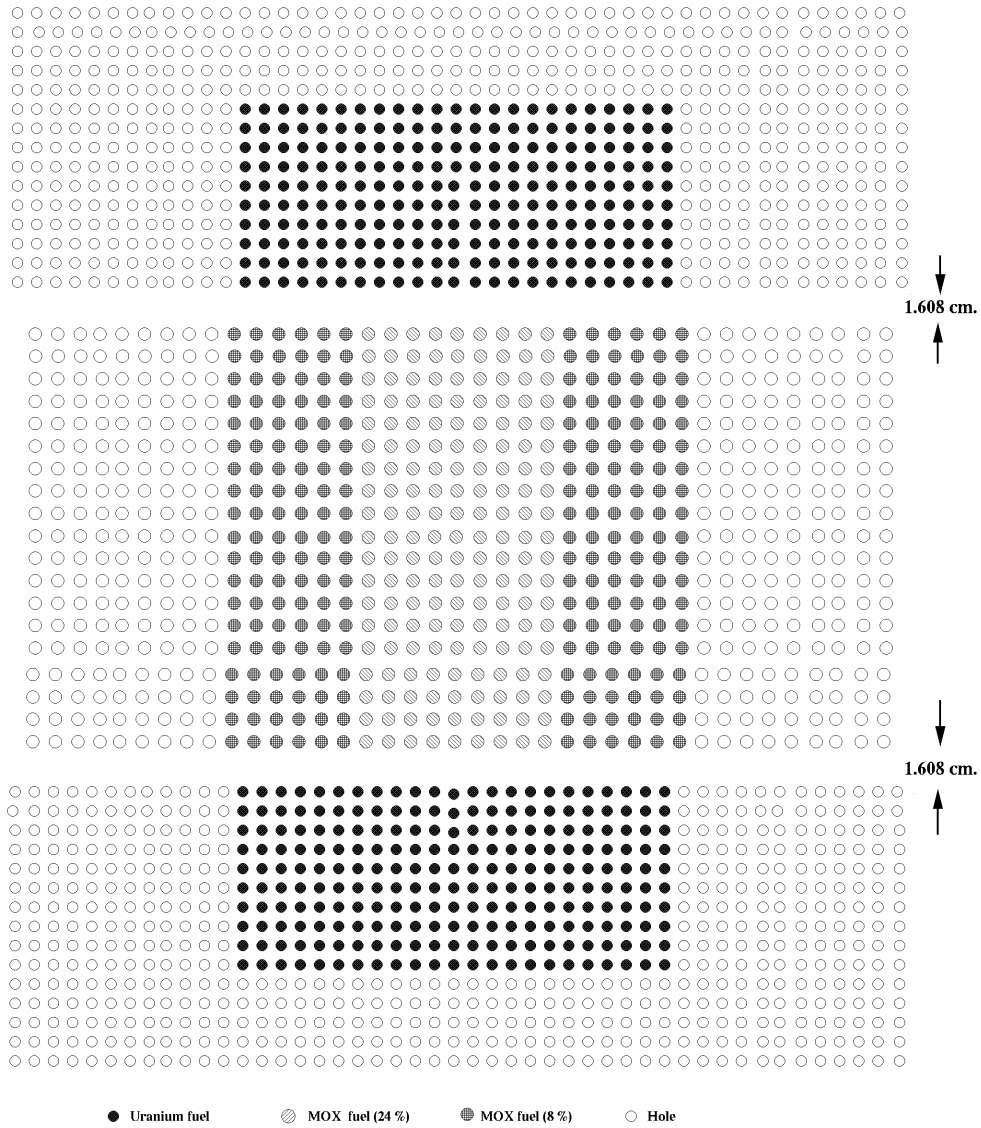

Fig. 30. A multiregion slab core configuration containing central traverse slabs of 8 wt % ^{240}Pu and 24 wt % ^{240}Pu fuels (19 × 21) and UO_2 outer regions (10 × 25).

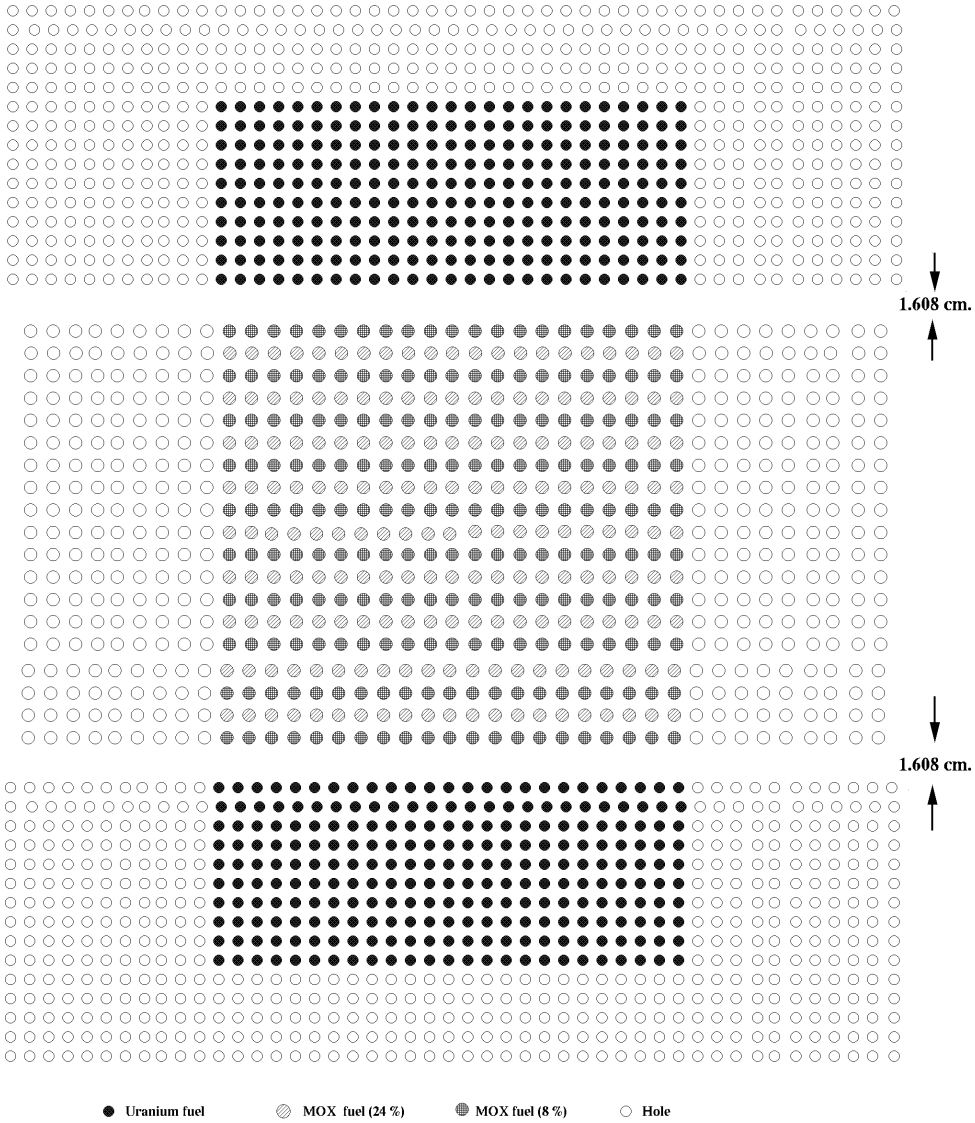

Fig. 31. A multiregion slab core configuration containing alternate rows of 8 wt % ^{240}Pu and 24 wt % ^{240}Pu fuels in the central slab region (19 × 21) and UO_2 outer regions (10 × 25).

1.3 Description of Fuel Rods

The experiments were performed using the MOX fuel rods obtained from Pacific Northwest National Laboratory (PNNL).[1] The MOX fuels used in the ESADA program were also used in two different sets of experiments at PNNL.[4,5] One series of experiments at PNNL in 1965 used both types of MOX fuels,[6,7] and later in 1975–1976 the 8 wt % ^{240}Pu fuels were used.[5]

The MOX fuel rod* length was 92.96 cm with a 91.44-cm active fuel length. The outer diameter of the fuel rod, including an 0.08-cm-thick Zircaloy-2 cladding, was 1.443 cm. Two plugs were welded on each side of the fuel rods. The total weight of the loaded fuel rod was 1340 g/rod with 1128 g of PuO_2-UO_2 per rod. The top end had 5 g of UO_2 powder. Dimensions of both MOX fuels were identical. A schematic representation of MOX fuel is given in Fig. 32.

The 2.72 wt % (actually 2.719 wt %) enriched UO_2 fuel was the third fuel used in these experiments. The UO_2 fuel was obtained from the U.S. Atomic Energy Commission-sponsored Large Reactor Development Program for comparison with the plutonium data and also for later use in multiregion experiments.[1]

The total weight of UO_2 fuel was 1028.02 g/rod with 905.93 g/rod of uranium. The weight of the ^{235}U was 24.63 g/rod. The UO_2 fuel rod length was 140.18 cm with a 121.92-cm active fuel length. The fuel pellet diameter was 1.016 cm. The outer diameter of the fuel rod was 1.196 cm. Fuel pellets were 1.52 cm in length. A schematic representation of the UO_2 fuel rod is given in Fig. 33. The MOX and UO_2 fuel rod specifications are summarized in Table 4.

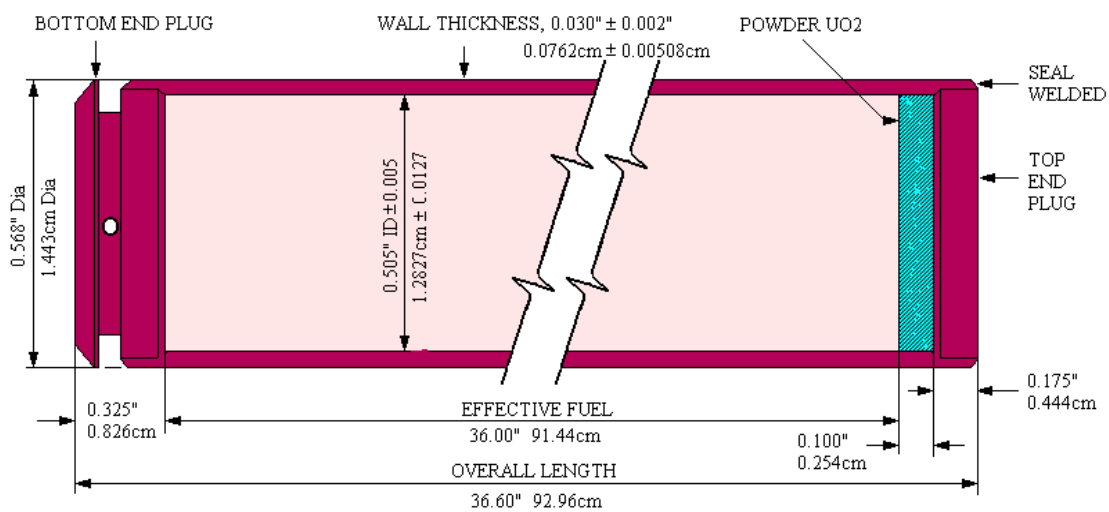

Fig. 32. MOX fuel rod.

*See the footnote in Sect. 3.2.

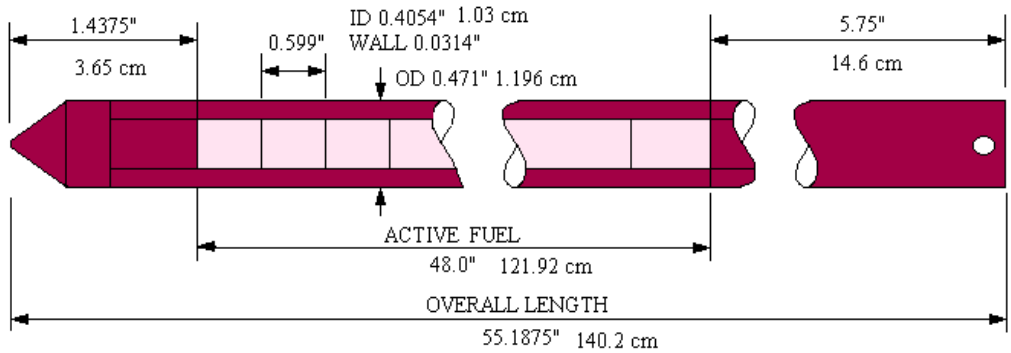

Fig. 33. Uranium fuel rod.

Table 4. The MOX and UO_2 fuel rod specifications

Parameter	MOX	UO_2
Pellet diameter, cm (in.)	1.2827 (0.505)	1.0160 (0.400)
Clad inner diameter, cm (in.)	No gap[a]	1.0297 (0.4054)
Clad outer diameter, cm (in.)	1.4427[1] (0.568)	1.1963 (0.471)[b]
Fuel length, cm (in.)	92.9540 (36.6)	140.1762 (55.1875)
Active fuel length, cm (in.)	91.4400 (36.0)	121.9200 (48.0)
Weight, g/rod	1128 PuO_2-UO_2	1028.02 UO_2
	22.56 PuO_2	905.93 U
	19.85 Pu	24.63 ^{235}U
Clad material	Zircaloy-2	Zircaloy-4

[a]The clad outer diameter was reported as 1.4427 cm (0.568 in.) in Ref. 1, but it was reported as 1.435 cm (0.565 in.) in all the other sources.[5–7] This difference in clad outer diameter is within the reported uncertainty for wall thickness. When the reported dimensions of the fuel outer diameter, clad outer diameter, and clad thickness given in Ref. 1 (which was also given in Fig. 32 of this document) are considered, it was assumed that there was a gap between fuel and clad. However, these fuels were vibratory compacted, and there was no gap between fuel and clad.[1,5–7] The MCNP calculations for core configurations with MOX fuel were performed assuming that there was a gap with a thickness of 0.004 cm between fuel and clad. Sensitivity calculations were performed for the gap present in the MCNP model. The maximum uncertainty in the k_{eff} value due to the considered gap was calculated as 0.046% for 8 wt % ^{240}Pu and 0.011% for 24 wt % ^{240}Pu MOX fuels (see Sect. 2.1.1 in Ref. 3).

[b]The clad outer diameters were reported as 1.196 cm (0.471 in.) and 1.1895 cm (0.4683 in.) in Ref. 1 (p. 125 and p. 123, respectively). Sensitivity calculations were performed for the difference in these reported clad outer diameters. The maximum uncertainty in the k_{eff} value due to this difference is calculated as 0.229% (see Sect. 2.2.1 in Ref. 3).

1.4 Description of Test Configurations

Several test positions were formed by removing the fuel rods at different locations. A uniformly distributed nine-rod pattern was arranged as a test configuration. These holes were filled with control rods or left as empty water holes. Also the reactivity worth of local voids was measured with voided aluminum tubes.

The isotopic composition of the control rod was 80% Ag, 15% In, and 5% Cd. For the reactivity worth measurement experiments with the salt-and-pepper core configuration, bare Ag-In-Cd control rods with an outer diameter of 1.0236 cm were used.

The isotopic composition of the control rod was 80% Ag, 15% In, and 5% Cd. For the reactivity worth measurement experiments with the salt-and-pepper core configuration, bare Ag-In-Cd control rods with an outer diameter of 1.0236 cm were used.

Also aluminum tubes were sealed to produce voids. The outer diameter of these aluminum tubes was 0.476 cm with 0.0559-cm thickness.

1.5 Description of Materials

Three different types of fuel rods were used during the experimental program. Two different MOX fuels and a low-enriched UO_2 fuel were used. MOX fuels were distinguished by the distribution of plutonium isotopes. The distributions of plutonium isotopes used in MOX fuel for the 8 wt % and 24 wt % ^{240}Pu fuels are given in Table 5.

Both MOX fuels contained 2.0 wt % PuO_2 in natural (0.72 wt % ^{235}U) UO_2. The total weight of a MOX fuel rod was 1128 g with 22.56 g/rod of PuO_2. Fuel density was reported as 9.54 g/cm^3 (Ref. 1). The percentages of the elements in the MOX fuel rods are given in Table 6.

Table 5. Isotopic composition of the metal plutonium in the MOX fuel rods

	Composition (wt %)	
Isotope[a]	8 wt % ^{240}Pu	24 wt % ^{240}Pu
^{239}Pu	91.615	71.762
^{240}Pu	7.654	23.503
^{241}Pu	0.701	4.080
^{242}Pu	0.030	0.656

[a]See the footnote in Sect. 3.3 of this document for ^{241}Am buildup.

Table 6. Percentages of the elements in the MOX fuel rods

Element	Composition (wt %)
PuO_2	2.0
UO_2	98.0
Pu metal	1.77
U metal	86.39
O	11.84

Zircaloy-2 was used as the cladding material for MOX fuel, but its composition is not reported in Ref. 1. During this work, the average values of weight fractions given in Ref. 8 are taken for the composition of Zircaloy-2. Density of Zircaloy-2 is taken as 6.56 g/cm^3. Isotopic composition of Zircaloy-2 clad is given in Table 7.

Table 7. Zircaloy-2 composition used for MOX fuel

Element	Composition (wt %)
Zr	98.27
Sn	1.45
Fe	0.13
Cr	0.10
Ni	0.05

A third fuel—2.72 wt % (2.719%) enriched UO_2—was also used. The total weight of the UO_2 was 1028.02 g/rod with 905.93 g/rod of uranium, and the weight of the ^{235}U was 24.63 g/rod. The fuel density was 95% of the theoretical density. A detailed chemical analysis* of UO_2 fuel is given in Table 8. The clad material for the UO_2 fuel rod was Zircaloy-4. Chemical analysis† of Zircaloy-4 is given in Table 9.

Table 8. Chemical analysis of UO_2 fuel

Isotope	2.72 wt % ^{235}U
U	88.15 wt %
C	<10 ppm
F	<10 ppm
Al	40 ppm
B	<0.5 ppm
Bi	<1 ppm
Cd	<0.3 ppm
Co	<4 ppm
Ca	9.5 ppm
Cr	34 ppm
Cu	2.0 ppm
Fe	266 ppm
In	<3 ppm
Mg	4.4 ppm
Mn	2.4 ppm
Mo	6.2 ppm
Ni	24.3 ppm
Pb	<8 ppm
Si	21 ppm
Sn	<2 ppm
Ti	3.9 ppm
V	<1 ppm
W	<50 ppm
N	<18 ppm
Zn	<8 ppm
O	Remainder

*See Table 15 in Sect. 3.3 for the UO_2 composition used in this evaluation.
†See Table 16 in Sect. 3.3 for the Zircaloy-4 composition used in this evaluation.

Table 9. Chemical analysis of Zircaloy-4 clad used for UO_2 fuel

Composition	Zircaloy-4
Zr	98.2 wt %
Sn	1.4 wt %
Fe	0.21 wt %
Cr	0.10 wt %
Ni	<0.004 wt %
C	95 ppm
Hf	<100 ppm
Al	<20 ppm
B	0.2 ppm
Cd	0.2 ppm
Co	10 ppm
Cu	33 ppm
Mg	<10 ppm
Mn	<20 ppm
Mo	<20 ppm
Pb	<20 ppm
Si	58 ppm
Ti	<20 ppm
V	<20 ppm
W	<50 ppm
N	45 ppm

No information was given on the type of aluminum used in these experiments.[1] During this study Al-6061 was assumed for the grid structure material. The density of aluminum is taken to be 2.7 g/cm^3. The characteristics of this type of aluminum are given in Table 10.[8]

Table 10. Isotopic distribution of Al-6061

Element	Composition (wt %)
Al	96.95
Mg	1.00
Fe	0.70
Si	0.60
Cu	0.25
Cr	0.20
Ti	0.15
Mn	0.15

Control rods composed of Ag-In-Cd were used for reactivity worth measurements. The isotopic composition of the control rod was provided in the earlier report,[1] but the density was not provided. The isotopic composition of these rods is given in Table 11.[1] The density of the control rod is taken as 9.75 g/cm^3.

Table 11. Isotopic composition of the Ag-In-Cd control rod

Element	Composition (wt %)
Ag	80
In	15
Cd	5

1.6 Supplemental Experimental Measurements

Two standard lattice plates were used during the experimental program. By changing the loading pattern, the standard lattice pitches were increased by a factor of $\sqrt{2}$ or 2. In this way, buckling measurement experiments were performed for five different lattice pitches. The number of reactivity worth measurements was increased by varying the test array materials and their positions.

The number of power distribution measurements in multiregion cores was increased by using additional core configurations. Measurements in concentric-region cores using different fuels and cores with interspersed fuels in a salt-and-pepper distribution were examined as different methods for extending the scope of the experimental program.

In addition to buckling, reactivity, and power distribution, heat rate measurements were performed during the program. In the heat rate experiments, thermally insulated and instrumented fuel rods were irradiated, and the temperature response was measured. After shutdown, these same rods were counted in the fuel rod gamma counter. The resulting ratio of heating rate to gamma activity provides a time-dependent "calorimetric" correction factor.

Using both uranium and plutonium fuels, heat rate experiments were conducted to correlate earlier power-to-gamma activity measurements made in the Saxton program.[9] Because fuel rods in this experiment were of different physical dimensions, new data were taken to reevaluate the time-dependent correction factors. Improved (over that used in Saxton) digital temperature measurements were taken by instrumenting the fuel rods during and after irradiation. The measurements of relative power distribution ratios of UO_2 vs 24 wt % ^{240}Pu, UO_2 vs 8 wt % ^{240}Pu, and 8 wt % ^{240}Pu vs 24 wt % ^{240}Pu are reported to be within 1% accuracy.

2. EVALUATION OF THE EXPERIMENTAL DATA

The effects of some of the uncertainties in the measured data on the k_{eff} value for some selected single-region core configurations were calculated using the ONEDANT code[10] with ENDF/B-IV 27 group cross sections with the homogenized lattice-cell fuel region. The homogenized lattice-cell cross-section sets for ONEDANT were prepared using the CSASIX[11] module of the SCALE code.

The sensitivity calculations for MOX fuels were performed only for selected single-region core configurations. Calculations were performed for five cases with different lattice pitches for the 8 wt % ^{240}Pu fuel and for two cases with different lattice pitches for the 24 wt % ^{240}Pu MOX fuels. The calculations were also performed for UO_2 fuel with two different lattice pitches.

The sensitivity calculations were performed basically for the uncertainties in the fuel characteristics (including uncertainties in the fuel density, dimensions, and fuel content), aluminum type, the composition of Zircaloy-2, and the reference plane for critical water height measurements. For MOX fuels the particle self-shielding effect was also considered. The parameters and the results of the sensitivity calculations are discussed in detail in Ref. 3.

For 8 wt % ^{240}Pu MOX fuel, the total uncertainties were calculated as 0.675%, 0.490%, 0.314%, 0.363%, 0.363%, and 0.556% for 1.7526-, 1.9050-, 2.4785-, 2.6942-, 3.5052-cm lattice pitches, respectively. For 24 wt % ^{240}Pu MOX fuel, total uncertainties were calculated as 0.371% and 0.413% for 2.4785- and 2.6942-cm lattice pitches, respectively. The fuel rod characterization parameters, especially uncertainty in clad thickness, were the parameters that yielded the largest uncertainty for 8 wt % ^{240}Pu, whereas ^{241}Am content was the parameter yielded the largest uncertainty for 24 wt % ^{240}Pu MOX fuel[3].

For UO_2 fuel the total uncertainties were calculated as 0.281% and 0.162% for 1.7526- and 2.4785-cm lattice pitches, respectively. In this case, the fuel rod characterization parameters, especially uncertainty in clad thickness, were the parameters that yielded the largest uncertainty.[3]

Also, the sensitivity calculation results show that the missing information in the report[1], the type of the aluminum used for grid materials, the Zircaloy-2 composition used as clad material, and reference plane for critical water height measurements, do not have large impacts on the k_{eff} value. The total uncertainties for these missing data are within the standard deviation (1 σ) of the results presented in Sect. 4 of this document.

3. BENCHMARK SPECIFICATIONS

3.1 Description of Model

Three different types of fuel rods were used during the experimental program. Two MOX fuels with different plutonium contents and a low-enriched UO_2 fuel were used. The fuel rods were inserted in a square lattice pitch. Two standard lattice pitches were available, and additional lattice pitches were achieved by changing the fuel-loading pattern. The reactivity worth of different materials and power distribution measurements were performed for multiregion core configurations with all available fuels. Installations of MOX fuel for the multiregion core configurations composed of two different MOX fuels are given in Fig. 1. Installation of MOX and UO_2 fuels for salt-and-pepper and slab array core configurations are given in Figs. 2 and 3, respectively. The fuel rods were supported by bottom, middle, and top aluminum grid plates, and the fuel rods rested on an aluminum plate.

3.2 Dimensions

Schematic diagrams of the MOX and UO_2 fuel rods are shown in Figs. 32* and 33. Also, the specifications of the MOX and UO_2 fuel rods are given in Table 4.

3.3 Material Data

The details of the atomic density calculations are given in Appendix A. Atomic densities for 8 wt % and 24 wt % ^{240}Pu MOX fuels are calculated using the weight fractions given in Tables 5 and 6. The total weight of the PuO_2-UO_2 was reported as 1128 g/rod, and the fuel density was reported as 9.54 g/cm^3. The calculated atomic number densities are given in Table 12.

---

*Although the fuel rods used in ESADA and PNNL experiments were the same, the dimensions were reported slightly differently in different sources. During this study, the dimensions reported in the ESADA document[1] are used. One of the reasons for this difference is due to the length of the UO_2 powder region. References 1 and 7 give the length of the fuel as 36.0 in., excluding the powder; however, Refs. 5 and 6 give the fuel length as 36.0 in., including powder region. Due to this difference in UO_2 powder length, the top plug was also reported differently in different sources. The top plug was reported as 0.444 cm (0.175 in.) in Refs. 1 and 7, whereas it was reported as 0.6985 cm (0.275 in.) in Refs. 5 and 6. Sensitivity calculations are performed to observe the sensitivity of the k_{eff} value to these differences in reported dimensions. For this purpose, the dimensions shown in Fig. 32 are modified so that the MOX fuel, UO_2 powder, and top end plug lengths are assumed as 90.94, 0.5, and 0.6985 cm, respectively. Sensitivity calculations show that the maximum uncertainty in the k_{eff} value due to these inconsistent dimensions is 0.060% (for 3.5052-cm lattice pitch) for 8 wt % ^{240}Pu fuel and 0.042% (for 2.4785-cm lattice pitch) for 24 wt % ^{240}Pu fuel (see Sect. 2.1.1 in Ref. 3 for detailed discussion).

Table 12. Atomic densities for the 8 wt % and 24 wt % ^{240}Pu MOX fuels

Element[a]	Atom density (atom/b-cm)	
	8 wt % ^{240}Pu	24 wt % ^{240}Pu
^{235}U	1.50490E-4	1.50490E-4
^{238}U	2.07511E-2	2.07511E-2
^{239}Pu	3.87455E-4	3.03494E-4
^{240}Pu	3.22350E-5	9.89834E-5
^{241}Pu	2.93999E-6	1.71115E-5
^{242}Pu	1.29476E-7	2.73988E-6
O	4.18019E-2	4.18019E-2

[a]The concentration of ^{241}Am in MOX fuels is not provided in Ref. 1. The ^{241}Am buildup is calculated as 0.0588 wt % (in 22 months) for 8 wt % ^{240}Pu and 0.267 wt % (in 17 months) for 24 wt % ^{240}Pu MOX fuel. During the sensitivity calculations, ^{241}Pu contents for both MOX fuels, given in Table 5, are also reduced. The maximum uncertainty in the k_{eff} value due to ^{241}Am buildup was calculated as 0.054% for 8 wt % ^{240}Pu and 0.248 wt % for 24 wt % ^{240}Pu MOX fuel (see Sect. 2.1.1 in Ref. 3).

The top UO_2 powder density was not reported in the original report.[1] The fuel density was reported as 9.54 g/cm^3, but it was not clear whether this density was for MOX only or for MOX plus UO_2 powder. It was reported that this layer is 5 g of UO_2 with a thickness of 0.254 cm. The UO_2 powder density is calculated as 15.23 g/cm^3 by using the reported weight and thickness, an unrealistic value[*]. Table 13 lists the atomic densities for the UO_2 powder using a density of 9.54 g/cm^3.

Table 13. Atomic densities for the UO_2 powder at the top of the MOX fuels

Element	Atom density (atom/b-cm)
^{235}U	1.55089E-4
^{238}U	2.11145E-2
O	4.25392E-4

Cladding material for MOX fuel was reported as Zircaloy-2, but the composition of Zircaloy-2 was not provided. Atomic densities for Zircaloy-2 are calculated by taking the weight fractions given in Table 7[†], and density is taken as 6.56 g/cm^3. Calculated atomic number densities are given in Table 14.

[*]Sensitivity calculations showed that the UO_2 powder density has negligible effect on k_{eff} value. The maximum uncertainty is calculated as 0.0009% (see Sect. 2.1.1 in Ref. 3).

[†]The effect of uncertainty in the Zircaloy-2 composition on the k_{eff} value was calculated by considering two extreme cases: (1) the maximum zirconium content with an isotopic composition of 98.65 wt % Zr, 1.20 wt % Sn, 0.07 wt % Fe, 0.05 wt % Cr, 0.03 wt % Ni; and (2) the minimum zirconium content with an isotopic composition of 97.89 wt % Zr, 1.70 wt % Sn, 0.20 wt % Fe, 0.15 wt % Cr, 0.06 wt % Ni. The composition yielding the maximum Δk_{eff} value is calculated as 0.016% (for 8 wt % ^{240}Pu MOX fuel with 3.5052-cm lattice pitch) using the maximum zirconium content (see Sect. 2.1.1 in Ref. 3).

Table 14. Atomic densities for the Zircaloy-2 clad used for MOX fuel

Element	Atom density (atom/b-cm)
Zr	4.25563E-2
Sn	4.82539E-4
Fe	9.19592E-5
Cr	7.59770E-5
Ni	3.36556E-5

The chemical composition of UO_2 fuel is given in Table 8. The fuel density was calculated as 10.40 g/cm^3 by using the 1.016-cm (0.400-in.) fuel rod diameter and the 121.92-cm (48.00-in.) fuel rod length with 1028.02 g/rod of UO_2. The atomic densities are calculated using the weights given in Ref. 1 rather than the given detailed chemical analysis. Although the uranium weight fraction is given as 88.15 wt % in Ref. 1 (p. 123), which was also given here in Table 8, different weight fractions are calculated with the given weights in Ref. 1. The uranium weight fraction was reported differently in two different places of Ref. 1. In Ref. 1, p. 123, the uranium weight fraction was given as 88.124 wt %, while it was reported as 88.15 wt % in the chemical analysis on the same page. Therefore, during this study, the weights reported in Ref. 1 are taken as basis instead of the given weight fractions. The weights and weight fractions along with the calculated atomic densities using 10.40-g/cm^3 fuel density for the UO_2 fuel are given in Table 15.

Table 15. Atomic densities for the UO_2 fuel

Element	Weight (g)	Weight fraction (wt %)	Atom density (atom/b-cm)
^{235}U	24.63	2.39587	6.38404E-4
^{238}U	881.30	85.7279	2.25545E-2
O	122.09	11.8762	4.64896E-2

Zircaloy-4 was used as the clad material for UO_2 fuel. The chemical analysis of Zircaloy-4 is given in Table 9. Atom densities for the impurities listed in Table 9 are not calculated. The density is taken as 6.56 g/cm^3, and the calculated atomic number densities are presented in Table 16.

Table 16. Atomic densities for the Zircaloy-4 clad

Element	Weight fraction (wt %)	Atom density (atom/b-cm)
Zr	98.286	4.25632E-2
Sn	1.400	4.65900E-4
Fe	0.210	1.48550E-4
Cr	0.100	7.59770E-5
Ni	0.004	2.69245E-6

The type of aluminum was not reported in Ref. 1, but Al-6061 is used in the benchmark calculations*. The density of aluminum is taken to be 2.7 g/cm^3. Isotopic composition of Al-6061 is given in Table 10. Calculated atomic densities for Al-6061 are given in Table 17.

*Sensitivity calculations are performed using 100% Al instead of Al-6061, and the maximum uncertainty is calculated as 0.062% for 8 wt % ^{240}Pu with a 3.5052-cm lattice pitch and 0.018 wt % for UO_2 fuel with a 2.4785-cm lattice pitch (see Sect. 2.1.2 for MOX fuel and Sect. 2.2.2 for UO_2 fuel in Ref. 3).

Table 17. Atomic densities for the Al-6061

Element	Atom density (atom/b-cm)
Al	5.84243E-2
Mg	6.68985E-4
Fe	2.03803E-4
Si	3.47361E-4
Cu	6.39681E-5
Cr	6.25420E-5
Ti	5.09388E-5
Mn	4.43946E-5

The density of water at 23° C is taken as 0.997518 g/cm^3. Atomic densities for water are given in Table 18.

Table 18. Atomic densities for water

Element	Atom density (atom/b-cm)
H	6.66898E-02
O	3.33449E-02

The multiregion experiments were performed using one boron concentration, 526 ppm. The details of the atomic density calculations for borated water are given in Appendix A. The calculated atomic densities for a 526-ppm boron concentration are presented in Table 19.

Table 19. Atomic densities for 526-ppm borated water

Boron concentration (ppm)	Density[a] (g/cm^3)	Element	Atom density (atom/b-cm)
526	0.998962	H	6.66733E-02
		O	3.33805E-02
		^{10}B	5.79484E-06
		^{11}B	2.39988E-05

[a]Borated water density (see Appendix A).

The density of air is taken as 1.20E-4 g/cm^3. The nitrogen and oxygen weight fractions are taken as 0.78 wt % and 0.22 wt %, respectively. The calculated atomic densities for air are given in Table 20.

Table 20. Atomic densities for air

Element	Atom density (atom/b-cm)
N	4.02428E-6
O	9.93684E-7

Table 21 gives the atomic densities for the Ag-In-Cd control rod using the weight fractions given in Table 11 and a density of 9.75 g/cm^3.

Table 21. Atomic densities for the control rod

Element	Atom density (atom/b-cm)
Ag	4.35461E-2
In	7.67055E-3
Cd	2.61167E-3

3.4 Temperature Data

No temperature data were specified in the original report.[1] Another report[12] indicated that these experiments were performed at 23°C.

4. RESULTS OF CALCULATIONS

All experimental configurations were modeled in detail using the MCNP-4A[13] Monte-Carlo code with both ENDF/B-V and ENDF/B-VI cross-section libraries. During the calculations, an S(α,β) thermal neutron scattering treatment was used for hydrogen in water.

The cases for concentric-region and salt-and-pepper core configurations were run with 450 generations of 4000 neutrons each, and the first 150 generations were skipped. Thus, the presented results for these core configurations are based on 1.2 million active histories with one standard deviation error, ranging from 0.0006 to 0.0007. The average CPU time for each run was approximately 10 h.

The multiregion slab core configurations were modeled in detail using the MCNP-4B with ENDF/B-V and ENDF/B-VI cross-section libraries. All cases were run with 650 generations of 7000 neutrons each, and the first 150 generations were skipped. Therefore, the presented calculational results are based on 3.5 million histories with one standard deviation error, ranging from 0.0004 to 0.0005. The average CPU time for each run was approximately 25 h.

The MCNP benchmark calculational results with ENDF/B-V and ENDF/B-VI cross-section libraries for salt-and-pepper core configurations are presented in Table 22. The MCNP benchmark calculational results for concentric-region core configurations are given in Table 23. The MCNP calculational results for multiregion slab core configurations are presented in Table 24. Because the core layout for case 23 was not given in the original report,[1] this case was excluded from the criticality calculations.

Table 22. MCNP calculation results for salt-and-pepper core configurations

Case No.	$k_{eff} \pm \sigma$ (ENDF/B-VI)	$k_{eff} \pm \sigma$ (ENDF/B-V)
1	0.99171 ± 0.0007	0.99576 ± 0.0007
2	0.99148 ± 0.0007	0.99774 ± 0.0007
3	0.99019 ± 0.0007	0.99582 ± 0.0007
4	0.99001 ± 0.0006	0.99623 ± 0.0007
5	0.98768 ± 0.0006	0.99272 ± 0.0007
6	0.99233 ± 0.0007	0.99770 ± 0.0007
7	0.99203 ± 0.0007	0.99778 ± 0.0007
8	0.99143 ± 0.0007	0.99614 ± 0.0006
9	0.99271 ± 0.0006	0.99667 ± 0.0006

Table 23. MCNP results for concentric-region core configurations

Case No.	$k_{eff} \pm \sigma$ (ENDF/B-VI)	$k_{eff} \pm \sigma$ (ENDF/B-V)
10	0.98835 ± 0.0007	0.99389 ± 0.0007
11	0.99190 ± 0.0007	0.99520 ± 0.0007
12	0.99028 ± 0.0007	0.99591 ± 0.0007
13	0.99031 ± 0.0007	0.99477 ± 0.0007
14	0.98817 ± 0.0007	0.99298 ± 0.0007
15	0.98797 ± 0.0006	0.99278 ± 0.0006
16	0.99266 ± 0.0007	0.99684 ± 0.0007
17	0.99572 ± 0.0006	1.00155 ± 0.0006

Table 24. MCNP calculation results for multiregion slab core configurations

Case No.	$k_{eff} \pm \sigma$ (ENDF/B-VI)	$k_{eff} \pm \sigma$ (ENDF/B-V)
18	0.99818 ± 0.0004	1.00309 ± 0.0004
19	0.99836 ± 0.0004	1.00324 ± 0.0005
20	0.99888 ± 0.0004	1.00394 ± 0.0004
21	0.99320 ± 0.0004	0.99871 ± 0.0004
22	0.99300 ± 0.0004	0.99820 ± 0.0004
24	0.98844 ± 0.0004	0.99320 ± 0.0004
25	0.98907 ± 0.0004	0.99332 ± 0.0004
26	0.99014 ± 0.0004	0.99391 ± 0.0004
27	0.99019 ± 0.0004	0.99562 ± 0.0004
28	0.99818 ± 0.0004	1.00309 ± 0.0004
29	0.99836 ± 0.0004	1.00324 ± 0.0005
30	0.99888 ± 0.0004	1.00394 ± 0.0004
31	0.98844 ± 0.0004	0.99320 ± 0.0004
32	0.98907 ± 0.0004	0.99332 ± 0.0004
33	0.99014 ± 0.0004	0.99391 ± 0.0004
34	1.00312 ± 0.0004	1.00773 ± 0.0004
35	1.00237 ± 0.0004	1.00716 ± 0.0005

5. REFERENCES

1. R. D. Leamer et al., *PuO_2-UO_2 Fueled Critical Experiments*, Westinghouse Electric Corporation, WCAP-3726-1, July 1967.
2. W. L. Orr, "Westinghouse Pu Recycle Experience and Design," *Proceedings of the Topical Meeting on The Plutonium Fuel Cycle*, May 1977.
3. H. Akkurt and N. M. Abdurrahman, *ESADA Plutonium Program critical Experiments: Single-Region Core Configurations*, ORNL/SUB/99-19SXZ175-1, February 1999.
4. V. O. Uotinen, B. R. Leonard, Jr., and R. C. Liikala, "The Neutronics of Plutonium Recycling," *Nuc. Tech.*, **18**, 115 (1973).
5. H.-K. Joo, *Rectangular Arrays of Water-Moderated UO_2-2 wt % PuO_2 (8 wt % ^{240}Pu) Fuel Rods*, NEA/NSC/DOC/95(03)/VI, Revision:0, OECD Nuclear Energy Agency (1997).
6. V. O. Uotinen, J. H. Lauby, L. C. Schmid, and W. P. Stinson, "Lattices of Plutonium-Enriched Rods in Light Water-Part I: Experimental Results," *Nuc. Tech.*, **15,** 257 (1972).
7. D. F. Newman, "Measurement of k_∞ and Relative Reaction Rates in an H_2O Moderated UO_2-PuO_2 Particulate Fueled Lattice," *Nuc. Tech.*, **15**, 192 (1972).
8. H. Etherington, *Nuclear Engineering Handbook*, 1st ed., McGraw-Hill Book Company, New York, (1958).
9. E. G. Taylor et al., *Saxton Plutonium Program- Critical Experiments for the Saxton Partial Plutonium Core*, Westinghouse Electric Corporation, EURAEC-1493, WCAP-3385-54, December 1965.
10. R. E. Alcouffe, R. S. Baker, F. W. Brinkley, D. R. Marr, R. D. O'Dell, and W. F. Walters, *DANTSYS: A Diffusion Accelerated Neutral Particle Transport Code System*, LA-12965-M, Los Alamos National Laboratory (1995).
11. N. F. Landers and L. M. Petrie, *CSAS: Control Module for Enhanced Criticality Safety Analysis Sequences*, NUREG/CR-0200, Vol. 1 Sect. C4, ORNL/NUREG/CSD/-2/V2/R6, Oak Ridge National Laboratory (1998).
12. L. C. Schmid et al., *Reactor Physics Data for The Utilization of Plutonium in Thermal Power Reactors*, BNWL-801, May 1968.
13. J. F. Briesmeister, *MCNP-A General Monte Carlo N-Particle Transport Code*, LA-12625-M, Los Alamos National Laboratory (1994).

Appendix A. ATOMIC NUMBER DENSITY CALCULATIONS

Atomic densities of the fuels are calculated using Avogadro's number and atomic weights from[*] using the following formula;

$$N_i = \frac{\rho w_e w_i N_A}{A_i} \quad ,$$

where

N_i = atom density of *i*th isotope,
ρ = density of mixture,
w_e = weight fraction of the element in the mixture,
w_i = weight fraction of the *i*th isotope in the element,
N_A = Avogadro's number,
A_i = atomic weight of the *i*th isotope.

The density of MOX fuel[1] is taken as 9.54 g/cm^3.

The H, O, ^{10}B, ^{11}B number densities are calculated by using the borated water density formula:[†]

$$\rho_{bwat} = \frac{0.997518 + C_B / 1000}{1 + C_B / 1920} \quad ,$$

where 0.997518 g/cm^3 is the density of water at 23°C, and ρ_{bwat} is the density (g/cm^3) of borated water by adding C_B grams of H_3BO_3 crystals to 1 L of water at 23°C.

The H_3BO_3 density in the borated water is calculated using the formula:[†]

$$\rho_{H_3BO_3} = \frac{C_B}{1000 \leftrightarrow (1 + C_B / 1920)} \quad .$$

The H_2O density in borated water is calculated using the formula:[†]

$$\rho_{H_2O} = \frac{997.518}{1000 \leftrightarrow (1 + C_B / 1920)} \quad .$$

The ^{10}B and ^{11}B atomic fractions in boron are 19.8 wt % and 80.2 wt %, respectively. Then, the fraction of boron in H_3BO_3 is calculated as:

$$f_B = \frac{(0.198 \leftrightarrow 10.0129 + 0.802 \leftrightarrow 11.0093)}{3 \leftrightarrow 1.0079 + (0.198 \leftrightarrow 10.0129 + 0.802 \leftrightarrow 11.0093) + 3 \leftrightarrow 15.9994} = 0.17485571 \quad .$$

C_B can be determined using the reported boron concentration p in parts per million and the formula:

$$C_B = \frac{997.518 \leftrightarrow p}{(f_B \leftrightarrow 10^6 - p)} \quad .$$

The H_3BO_3 and H_2O densities are calculated by substituting the calculated C_B value into the equations given above. Then, the boron number density is calculated with H_3BO_3 density, ^{10}B and ^{11}B

---

[*]F. W. Walker, J. R. Parrington, and F. Feiner, **Nuclides and Isotopes,** 14th Ed., General Electric Nuclear Energy Operations, 1989.

[†]H.-K. Joo, *Rectangular Arrays of Water-Moderated UO_2-2 wt % PuO_2 (8 wt % ^{240}Pu) Fuel Rods*, NEA/NSC/DOC/ 95(03)/VI, Revision 0, OECD Nuclear Energy Agency (1997).

atomic fractions, and Avogadro's number. The H and O number densities are calculated by summing the atomic number densities from H_2O and H_3BO_3.

The multiregion measurements are performed using 526-ppm boron concentration. The calculated values of C_B, ρ_{bwat}, $\rho_{H_3BO_3}$ and ρ_{H2O}, for 526-ppm boron concentration are summarized in Table A.1. The calculated number densities using these values were given in Table 41 in Sect. 3.3.

Table A.1. The calculated values of the C_B and the densities for the specified boron concentrations

Parameter	526 ppm
C_B, g	3.00978
ρ_{bwat}, g/cm^3	9.98962E-1
$\rho_{H_3BO_3}$, g/cm^3	3.00507E-3
ρ_{H_2O}, g/cm^3	9.95957E-1

REFERENCE

1. R. D. Leamer et al., *PuO_2-U_2 Fueled Critical Experiments*, Westinghouse Electric Corporation, WCAP-3726-1, July 1967.

<u>REVIEW ADDENDUM</u>: *ORNL/SUB/00-XSZ175V-1*
by R. J. Ellis

"Neutronics Benchmarks for the Utilization of Mixed-Oxide Fuel: Joint U.S./Russian Progress Report for Fiscal Year 1997: Volume 4, Part 5—ESADA Plutonium Program Critical Experiments: Multi-Region Core Configurations" by Hatice Akkurt & Naeem M. Abdurrahman.

I reviewed this report in August 1999 and at that time provided to the authors my comments, suggestions, and corrections directly in the text of my copy. In this addendum, I address some of the issues pertaining specifically to the MCNP models and results presented in the report. I make some reference to MCNP calculations[a,b] I performed while I was with AECL. These were large difficult-to-converge (because of the D_2O) cases for which I developed modeling and statistical methods.

The ESADA experimental configurations were modeled using two versions of MCNP (the <u>M</u>onte <u>C</u>arlo <u>N</u>-<u>P</u>article transport code): MCNP-4A and MCNP-4B[c]. The MCNP calculations were performed using nuclear data libraries based on ENDF/B-V, and on ENDF/B-VI cross sections.

MCNP-4A was released in November 1993, and amongst its improvements were an enhanced statistical analysis, distributed processor multi-tasking for parallel running, improved criticality output, and better modeling capabilities. MCNP-4B was released in March 1997 and features differential operator perturbations, enhanced photon physics, enhanced neutron lifetimes, and other modeling improvements.

These MCNP cases were performed with 7000 histories per cycle (run) with a total of 650 cycles per case; the first 150 cycles of each case were skipped generations. Akkurt mentions that based on the 3.5×10^6 active histories per case, the standard deviation for k_{eff}-determinations ranges from 0.0004 to 0.0005; the approximate rule-of-thumb for MCNP KCODE calculation uncertainties would suggest an error of about $\pm1/(3.5\times10^6)$ is equal to 0.000535.

Tables 22-24 in the report present the MCNP results for the 35 multi-region ESADA core configuration critical experiments. MCNP-4A results are shown in Tables 22 and 23 for the salt and pepper core configurations, and the concentric region core configurations, respectively. MCNP-4B was used to calculate the k_{eff}-values shown in Table 24 for the slab core configurations. For all these sets of results, the findings are tabulated for both the ENDF/B-V and ENDF/B-VI nuclear data libraries. For the salt and pepper core configurations, the average ENDF/B-VI k_{eff} determination is 0.99106±0.00055 and the average ENDF/B-V calculation is 0.99628±0.00056. For the concentric region core configurations, the average results are 0.99067±0.00101 and 0.99549±0.00106, respectively, for ENDF/B-VI and ENDF/B-V. Both of these sets of results were calculated with MCNP-4A. MCNP-4B was used to simulate the multi-region slab core configurations. Using ENDF/B-VI data, the average k_{eff} was 0.99459±0.00129 compared to 0.99934±0.00133 for ENDF/B-V.

For the three sets of ESADA reactor configurations, the k_{eff} results from MCNP using the nuclear data libraries based on ENDF/B-V are closer to 1 than the results based on ENDF/B-VI libraries. For all the classes of results with MCNP-4A and MCNP-4B, there is a clear reactivity offset in k_{eff} is about 0.0050 higher for the ENDF/B-V results. Another observation is that the critical k_{eff} determinations with MCNP-4B are about 0.0039 higher than the corresponding MCNP-4A results.

Nuclear data libraries have a large effect on MCNP k_{eff} determinations. The particular version of ENDF/B-VI has a bearing on ultimate results. Release 4 is supposed to be the best one. Earlier versions might have some deficiencies in some of the cross sections, U in particular.

One item that has a bearing on the k_{eff} determinations with MCNP is the boron concentration in the coolant. In Appendix A, the denominator of the expression for C_B is not correct. It should be $f_B(10^6\text{-p})$. As a consequence, the value for C_B in Table A.1 corresponding to 526-ppm boron should be 3.00231 g instead of 3.00978 g.

All the salt and pepper core configurations and the concentric region core configurations were clean cores containing no boron. Only certain cases (24-27, 31-33) of the multi-region slab core configurations used boronated water at 526-ppm boron. It is presumed that the correct amount of boron was used in the MCNP models, despite the error in C_B in Table A.1. However, if the boron levels were out by a proportionate error, then the k_{eff} determinations would be too low by a very small amount (ranging from 0.00008 for LEU to about 0.00003 for RG MOX). It is interesting to note that as a subset, the average k_{eff} values for the boronated cases are considerably lower than the averages for the other slab core configuration cases:

1. Avg k_{eff} for the ENDF/B-VI boronated cases = 0.98936; Avg k_{eff} for the other ENDF/B-VI cases = 0.99792; reactivity difference = -0.867%
2. Avg k_{eff} for the ENDF/B-V boronated cases = 0.99378; Avg k_{eff} for the other ENDF/B-V cases = 1.00288; reactivity difference = -0.913%

Another modeling issue that has to be considered in MCNP KCODE calculations of k_{eff} is the need for a correction for the coolant temperature from the library temperature to the actual experimental temperature. Thermal scattering kernels are only available in MCNP at specific temperatures, so the calculations performed for this report were done for a nominal coolant temperature. It is assumed that the coolant density (number densities) is appropriately adjusted to account for the correct thermal expansion. The remaining discrepancy would be due to neutron thermalization. The assumption on page 48 is that the experimental temperature is 23°C. This is not the actual temperature for the nuclear data. As an example of temperature effects, critical calculations for CANDU fuel bundles in the ZED-2 reactor required a k-correction of +0.0004 to account for a 3° temperature defect. It is assumed these effects will be quite small for the ESADA core configurations.

Another modeling deficiency in MCNP is that delayed neutrons are assumed in MCNP to be born with the same neutron energy spectrum as fission neutrons (i.e., the delayed neutrons are explicitly included in the total ν) though their actual birth energy averages to about 300-400 keV. Depending on the actual reactor, the delayed neutron energy effect can necessitate a small change to calculated k_{eff} values.

The triple-covariance-weighted "three-combined k_{eff}" is the best final estimate from an MCNP calculation[d]. This answer is a combination of the three individual k_{eff} estimators. The three different estimators for k_{eff} are the collision estimator, the absorption estimator, and the track length estimator. The confidence interval based on the three statistically combined k_{eff} estimator is the recommended result to use for all final k_{eff} confidence interval quotations because all of the available information has been used in the final result. The three k_{eff} estimators are correlated, not independent. The combined k_{eff} is computed using a maximum likelihood estimate. The technique is a generalization of the inverse variance weighting for uncorrelated estimators, and produces the maximum likelihood estimate for the combined average k_{eff}. It is the "almost-minimum" variance estimate[e].

This method of combining estimators gives the best estimate to use for a final k_{eff}; sometimes (for highly positively correlated estimators) it is seen that this correct answer is outside of the interval defined by the individual average estimates. This type of behavior occurs with high positive correlation because if one estimator is above or below the expected value, the other estimators have a good probability of being on the same side of the expected value.

In performing MCNP criticality k_{eff} determinations with KCODE, calculating a large number of histories does not guarantee a precise result. One has to be careful of using a brute force approach. Stable errors should decrease by $(1/\sqrt{N})$ but the fission source has to settle in order for the results to become stable. The number of histories per cycle must be large to reduce negative biases in k_{eff} inherent to Monte Carlo methods[f]. To obtain a stable "settled" fission source distribution, a series of MCNP calculations is recommended: initially, 20 cycles of 100 histories each, then the batch size is increased by a factor of about 2.5 for subsequent cases. This is continued until the batch size is at least 10000 histories per cycle. Then, cases with 35 active cycles (5 inactive cycles are disregarded at the start of each case). A floating average of the final results of three or five of these 35-cycle cases is monitored to ensure stability in the average value. Once stability is seen (no steady increase or decrease in the average value of k_{eff}) then at least 15 (or more) case results are treated as a set.

The final result is the weighted mean of numerous (N) case studies. The uncertainty indicated is the larger of the internal or external errors. The internal error is the square root of the reciprocal of the sum of the squares of the individual case uncertainties. The external error is the weighted standard deviation. The ratio of external error to internal error is called the Birge ratio: it is a statistical measure of the goodness of the data. Statistically, the Birge ratio should be in the range $1\pm(2f)^{-0.5}$ where f=N-1 is the number of degrees of freedom.

In summary, the k_{eff} results for the three sets of MCNP calculations for the multi-region ESADA critical core configurations are self-consistent and agree fairly well with experiment. These cores are quite heterogeneous and it is assumed that the corresponding MCNP models must be quite detailed and carefully constructed. There may be small corrections required to the k_{eff} results to compensate for:

1. the actual experimental moderator temperature vs the MCNP standard temperature
2. the lower energy of delayed neutrons vs the fission neutron spectrum
3. possibly slightly too much boron in some of the models.

There are a some effects seen related to the use of MCNP-4A or MCNP-4B that are similar in magnitude when either ENDF/B-V or ENDF/B-VI nuclear data libraries are used. Furthermore, there are reactivity effects observed between MCNP cases with ENDF/B-V and ENDF/B-VI similar in magnitude for either MCNP-4A or MCNP-4B runs. The changes in coding from MCNP-4A to MCNP-4B are not large with respect to internal calculations, mostly just some improvements to the modeling capabilities, such as repeated geometry options. The small differences in the k_{eff} determinations when using MCNP-4A or MCNP-4B are more likely related to differences in nuclear data libraries and different releases of ENDF/B-V and ENDF/B-VI (and perhaps effects related to problems with unresolved resonance cross sections for ^{238}U). The apparent sizeable deficit in k_{eff} for the boronated cases of the multi-region slab configuration cores (about 0.9% reactivity) may be a modeling artifact.

a) R.J. Ellis, "MCNP Analysis of 37-Element UO2 Bundle Core Measurements in ZED-2", Reactor Technology Branch report RTB-TN-010, September 1994.

b) J.V. Donnelly and R.J. Ellis, "Monte Carlo Analysis of ZED-2 Substitution Measurements of Low-Void-Reactivity CANDU Fuel", Research Technology Branch report RTB-TN-038, February 1995.

c) J.F. Briesmeister, ed., "MCNP – A General Monte Carlo N-Particle Transport Code – Version 4B", Los Alamos National Laboratory report LA-12625-M, Version 4B, UC 705 and UC 700, March 1997.

d) T.J. Urbatsch, R.A. Forster, R.E. Prael, and R.J. Beckman, "Estimation and Interpretation of k_{eff} Confidence Intervals in MCNP," Los Alamos National Laboratory report LA-12658, November 1995.

e) M. Halperin, "Almost Linearly-Optimum Combination of Unbiased Estimates," Amer. Stat. Ass. J., **56**, 36-43 (1961).

f) R.J. Brissenden and A.R. Garlick, "Biases in the Estimation of k_{eff} and its Error by Monte Carlo Methods", Annals of Nuclear Energy, **13**, Number 2, pp. 63-83, 1986.

INTERNAL DISTRIBUTION

1–5. B. B. Bevard
6. J. J. Carbajo
7. E. D. Collins
8. B. S. Cowell
9. M. D. DeHart
10. F. C. Difilippo
11. R. J. Ellis
12–16. J. C. Gehin
17. S. R. Greene
18. T. W. Horning
19. D. T. Ingersoll
20. M. A. Kuliasha
21. G. E. Michaels
22. B. D. Murphy
23. D. L. Moses
24. C. V. Parks
25–29. R. T. Primm III
30. C. C. Southmayd
31. Central Research Library
32–33. ORNL Laboratory Records (OSTI)
34. ORNL Laboratory Records–RC

EXTERNAL DISTRIBUTION

35. N. Abdurrahman, College of Engineering, Dept. of Mechanical Engineering, University of Texas, Austin, Texas 78712
36. M. L. Adams, Department of Nuclear Engineering, Texas A&M University, Zachry 129, College Station, TX 77843
37–39. H. Akkurt, 2919 Cooley Building, 2355 Bonisteel Boulevard, Ann Arbor, MI, 48109-2104
40. D. Alberstein, Los Alamos National Laboratory, MS-E502, P.O. Box 1663, Los Alamos, NM 87545
41. J. Baker, Office of Fissile Materials Disposition, U.S. Department of Energy, MD-3, 1000 Independence Avenue SW, Washington, DC 20585
42. J. B. Briggs, Idaho National Environmental and Engineering Laboratory, P.O. Box 1625-3855, Idaho Falls, ID 83415-3855
43. L. Holgate, Office of Fissile Materials Disposition, U.S. Department of Energy, MD-1/2, 1000 Independence Avenue SW, Washington, DC 20585
44. N. Fletcher, Office of Fissile Materials Disposition, U.S. Department of Energy, MD-3, 1000 Independence Avenue SW, Washington, DC 20585
45. K. Chidester, Los Alamos National Laboratory, MS-E502, P.O. Box 1663, Los Alamos, NM 87545
46. W. Danker, U.S. Department of Energy, MD-3, 1000 Independence Avenue SW, Washington, DC 20585
47. T. Gould, Lawrence Livermore National Laboratory, P.O. Box 808, MS-L186, Livermore, CA 94551
48. L. Jardine, Lawrence Livermore National Laboratory, P.O. Box 808, MS-L166, Livermore, CA 94551
49. Dr. Alexander Kalashnikov, Institute of Physics and Power Engineering, 1 Bondarenko Square, Obninsk, Kaluga Region, Russia 249020
50–54. D. E. Klein, Associate Vice Chancellor for Special Engineering Programs, The University of Texas System, 210 West Sixth Street, Austin, TX 78701
55. J. O. Nulton, Office of Fissile Materials Disposition, U.S. Department of Energy, MD-3, 1000 Independence Avenue SW, Washington, DC 20585
56. S. L. Passman, Sandia National Laboratories, Suite 110, 950 L'Enfant Plaza, S.W., Washington, DC 20024-2123

57–61. Dr. Alexander Pavlovitchev, Russian Research Center "Kurchatov Institute," Institute of Nuclear Reactors VVER Division, VVER Physics Department, 123182, Kurchatov Square, 1, Moscow, Russia

62. K. L. Peddicord, Associate Vice Chancellor, Texas A&M University, 120 Zachry, College Station, TX 77843-3133

63. G. Radulescu, Framatom Cogema Fuels, 1261 Town Center Drive, MS-423, Las Vegas, Nevada 89143

64. W. D. Reece, Texas A&M University, Department of Nuclear Engineering, Zachry 129, College Station, TX 77843-3133

65. P. T. Rhoads, Office of Fissile Materials Disposition, U.S. Department of Energy, MD-4, 1000 Independence Avenue SW, Washington, DC 20585

66. J. Thompson, Office of Fissile Materials Disposition, U.S. Department of Energy, MD-4, 1000 Independence Avenue SW, Washington, DC 20585

67. F. Trumble, Westinghouse Savannah River Company, Building 730R, Room 3402, WSRC, Aiken, SC 29808

68. R. H. Clark, Duke/Cogema/Stone & Webster, 400 South Tryon Street, WC-32G, P.O. Box 1004, Charlotte, NC 28202

69. S. Nesbit, Duke/Cogema/Stone & Webster, 400 South Tryon Street, WC-32G, P.O. Box 1004, Charlotte, NC 28202

70. D. Dziadosz, Innsbruck Technical Center, 5000 Dominion Blvd., Glen Allen, VA 23060

71. M. S. Chatterton, Office of Nuclear Reactor Regulation, MS O10B3, U.S. Nuclear Regulatory Commission, Washington, DC 20555-0001

72. U. Shoop, Office of Nuclear Reactor Regulation, MS O10B3, U.S. Nuclear Regulatory Commission, Washington, DC 20555-0001

73. J. P. Halloway, 2919 Cooley Building, 2355 Bonisteel Boulevard, Ann Arbor, MI 48109-2104